Received: 29 October 2021 | Revised: 11 March 2022 | Accepted: 14 March 2022

DOI: 10.1002/jbm.b.35069

RESEARCH ARTICLE

Synthesis of a novel monofilament bioabsorbable suture for biomedical applications

Kara M. de la Harpe | Thashree Marimuthu | Pierre P. D. Kondiah | Pradeep Kumar | Philemon Ubanako | Yahya E. Choonara

Wits Advanced Drug Delivery Platform Research Unit, Department of Pharmacy and Pharmacology, School of Therapeutic Sciences, Faculty of Health Sciences, University of the Witwatersrand, Parktown, Johannesburg, South Africa

Correspondence
Yahya E. Choonara, Wits Advanced Drug Delivery Platform Research Unit, Department of Pharmacy and Pharmacology, School of Therapeutic Sciences, Faculty of Health Sciences, University of the Witwatersrand, 7 York Road, Parktown, 2193, Johannesburg, South Africa.
Email: yahya.choonara@wits.ac.za

Funding information
National research Foundation (NRF)

Abstract

In this research, a novel bioabsorbable suture that is, monofilament and capable of localized drug delivery, was developed from a combination of natural biopolymers that where not previously applied for this purpose. The optimized suture formulation comprised of sodium alginate (6% wt/vol), pectin (0.1% wt/vol), and gelatin (3% wt/vol), in the presence of glycerol (4% vol/vol) which served as a plasticizer. The monofilament bioabsorbable sutures where synthesized via in situ ionic crosslinking in a barium chloride solution (2% wt/vol). The resulting suture was characterized in terms of mechanical properties, morphology, swelling, degradation, drug release, and biocompatibility, in addition to Fourier-transform infrared (FTIR) spectroscopy, Powder X-ray Diffraction (PXRD) and Differential Scanning Calorimetry (DSC) analysis. The drug loaded and non-drug loaded sutures had a maximum breaking strength of 4.18 and 4.08 *N*, in the straight configuration and 2.44 *N* and 2.59 *N* in the knot configuration, respectively. FTIR spectrum of crosslinked sutures depicted $\Delta 9\ cm^{-1}$ downward shift for the carboxyl stretching band which was indicative of ionic interactions between barium ions and sodium alginate. In vitro analysis revealed continued drug release for 7 days and gradual degradation by means of surface erosion, which was completed by day 28. Biocompatibility studies revealed excellent hemocompatibility and no cytotoxicity. These results suggest that the newly developed bioabsorbable suture meets the basic requirements of a suture material and provides a viable alternative to the synthetic polymer sutures that are currently on the market.

KEYWORDS
bioabsorbable suture, localized drug delivery, monofilament, sodium alginate

1 | INTRODUCTION

Biopolymers have inimitable potential to revolutionize the biomedical field, but their application is often limited by their insufficient tensile strength and poor mechanical properties. In terms of the surgical field,

[Correction added on 4 May 2022, after first online publication: Copyright statement has been updated.]

biopolymers have led to several new and useful medical devices such as bio-adhesives, new wound dressing materials and drug-eluting stents.[1] Yet, synthetic suture materials, which represents some of the most employed types of medical devices, have yet to see a biopolymer-based clinical counterpart.[2] Herein we describe a novel suture material that consists of three carefully selected biopolymers that are expertly combined to produce a bioabsorbable suture that, not only meets the United States Pharmacopeia's requirements for suture tensile strength, but also acts as a localized drug delivery device.

Synthetic sutures are notorious for causing significant foreign body reactions and having extensive degradation profiles that continue long after wound healing is complete.[3] Naturally derived polymers, having excellent biocompatibility, impressive biodegradation properties and close similarity to the native extracellular matrix, can help improve these shortcomings of synthetic sutures.[4] Through the course of this study, several biopolymers were investigated for their potential to yield strong, yet flexible bioabsorbable sutures with mechanical properties that are equivalent to that of synthetic sutures currently found on the market. Alginate, a natural polysaccharide found in various microalgae, was selected as base material. This selection hinged not only on the well-known favorable properties of the biopolymer (i.e., non-toxic, biocompatible, biodegradable, biostable and hydrophilic) but also on its instantaneous crosslinking in the presence of various multivalent cations. This straightforward crosslinking process avoids the use of harsh inorganic solvents, does not alter the inherent biocompatibility of the biopolymer structure and allows for safe and timely degradation. Yet, crosslinked alginate on its own does not possess the qualities necessary to stand on even footing with synthetic sutures. Additional strength and elasticity must be obtained for the biopolymer structure to meet the requirements of modern surgery. Pectin is a complex, crystalline heteropolysaccharide found ubiquitously in plant cell walls. Pectin and alginate are very similar in structure and have been classified as synergistic biopolymers that display greater mechanical performance combined, than individually.[5] Through the addition of pectin to the bioabsorbable suture formulation, higher load failure (N) and tensile strength (N/mm^2) were obtained, bringing the biopolymer structure closer to its synthetic equivalents. The problem of elasticity was overcome by the addition of glycerol, which serves as a biocompatible plasticizer. Glycerol as a plasticizer provides a stable and flexible suture system endowed by its ability to form H-bonds via its inherent hydroxy moieties.[6] Yet, the mechanical performance of the bioabsorbable suture was still not on par with that of marketed synthetic sutures. This was, however, dramatically changed through the introduction of gelatin to the bioabsorbable suture formulation, which increased both the strength and elasticity of the biopolymeric structure. Gelatin, in contrast to the previous two polysaccharides, is a protein that is closely derived from collagen and therefore owns a close structural and molecular similarity to extracellular matrix proteins.[7] The gelatin-polysaccharide combination has been described as a promising approach to the development of superior biomaterials and found to be stable, have great mechanical resilience, and low thermal expansion, in addition to antimicrobial, anti-inflammatory and wound healing properties.[8]

Suture performance is of paramount importance when it comes to the successful outcome of surgical procedures, such as microvascular surgery (MVS). If the suture material breaks prematurely, induces thrombosis, or triggers severe inflammatory responses, through the course of MVS, vessel patency might be compromised with severe consequences (e.g., tissue necrosis, flap or transplant failure) for the patient. Additionally, MVS is plagued by routine complications, such as ischemic reperfusion injury (IRI) and the dreaded "no-reflow" phenomenon that has been reported to occur in up to 60% of percutaneous coronary interventions, 58% of failed digital replantation surgeries and a staggering 82% of free flap transfers.[9–11] IRI is inevitable in most cases of MVS, due to the ischemic nature of the procedure, where blood flow is interrupted with small vascular claps, which causes inflammatory cells, toxic metabolites, and reactive oxygen species to accumulate in the vessel, proximal to the clamp. Once the clamps are removed and the blood flow restored, the influx of inflammatory mediators can cause immediate and irreversible tissue damage or progressive clogging of the vessel lumen. This obstruction of the vessel lumen is known as the no-reflow phenomenon and often slips by unnoticed until vessel patency is compromised several days postsurgery.[12]

Sutures as drug delivery devices, pose several unequaled benefits that include localized drug delivery, which avoids the risk of systemic side effects, lowers the amount of drug needed, and decreases the overall cost of treatment. Additionally, since sutures are already used in most medical procedures, there is no need to introduce a second foreign object to the surgical field, thereby lowering the chances of infection, while saving the surgeon valuable time.[2] Moreover, continued hospitalization is not necessary to achieve sustained drug administration and if the suture material is absorbable, a second procedure to remove the drug delivery device is not necessary, which again saves time and money, but also spares the patient unnecessary pain and discomfort.[13] Dexamethasone (DEX), a potent anti-inflammatory drug, has been shown to prevent IRI and no-reflow on a microvascular level, if administered in high concentrations at the onset of reperfusion. Systemic delivery of high concentrations DEX, can however lead to unwanted side effects such as immunosuppression, which could increase the risk of nosocomial infections and inhibit effective wound healing.[14] Localized delivery of DEX, directly to the cite of injury, where the risk of IRI and no-reflow is highest, by means of a suture material could provide a viable, and potentially safer and more effective alternative, for the prevention of these complications during MVS.

The objective of this study was, therefore, to combine and crosslink the biopolymers discussed here, in such a way that they yield a novel bioabsorbable suture with excellent mechanical properties, good thermal stability, and ideal degradation behavior. Additionally, we set out to coat the newly fabricated bioabsorbable suture in a lipid-drug layer that will allow for immediate and sustained DEX release over a period of approximately 7 days, in order to attenuate the occurrence of IRI and the no-reflow phenomenon in MVS.

TABLE 1 Composition of the optimized biopolymeric suture formulation

Component	Sodium alginate	Pectin	Gelatin	Glycerol
Concentration	6% (wt/vol)	0.1% (wt/vol)	3% (wt/vol)	4% (vol/vol)

2 | EXPERIMENTAL

2.1 | Materials

Biopolymers and pharmaceutical materials comprising of Sodium alginate (M/G ratio, 1.45), pectin from citrus peel (degree of esterification, 86.44%), gelatin (pharmaceutical grade, no. 48723, type B), dexamethasone powder (bioreagent, suitable for cell culture, ≥97%), collagen and Triton X-100 and cell culture reagents namely; Dulbecco's minimal essential medium (DMEM), fetal calf serum (FCS), antibiotics (100 IU/ml penicillin and 100 IU/ml streptomycin) were sourced from Sigma-Aldrich (Missouri, USA). Barium chloride dihydrate and glycerol, MW = 92.1 g/mol) was purchased from LabChem (Founder's hill, Johannesburg, SA). Phosphate buffered saline (PBS) tablets and ethanol were sourced from Rochelle Chemicals (Electron, Johannesburg, SA). Phosphatidyl choline (from soybean, <99% TLC) was procured from Avanti Polar Lipids Inc (Alabaster, Alabama, USA). Human whole blood was collected into sodium citrate anticoagulation tubes, from healthy volunteers (ethical clearance number: M180978). Human embryonic kidney cells (HEK 293) were purchased from Cellonex (Johannesburg, South Africa).

2.2 | Synthesis of the bioabsorbable suture

Various biopolymers, in different concentrations and ratios, were considered for inclusion in the bioabsorbable suture. Alginate was selected as the primary biopolymer, based on its ability to form suture-like strings after extrusion and crosslinking, and acted as the basis of the polymer matrix. Observations that were made during the preliminary development phase is summarized in Tables S1 and S2, while Figure S1, shows the suture-like stings that were produced with different concentrations of alginate.

The optimized bioabsorbable suture formulation consisted of three biopolymers namely, alginate, pectin and gelatin, which were individually dissolved in deionized water and then combined with the plasticizer, glycerol, to obtain the optimized concentration of each component, (Table 1). The resulting hydrogel was homogenized for 15 min, to ensure even distribution of the components throughout, followed by 5 min of sonication with a bath ultrasonicator (Labotec, Midrand, SA), to remove unwanted air bubbles. The hydrogel was carefully loaded into a 5 ml luer lock syringe fitted with a 23G needle and extruded into a crosslinker bath containing $BaCl_2$ at an optimized concentration of 2% (wt/vol). Extrusion of the monofilament bioabsorbable suture was performed with the aid of Texture Analyser (TA, XT plus, Stable Micro Systems, England) equipped with a universal syringe rig, to ensure uniformity, consistency, and reproducibility in the bioabsorbable suture morphology and diameter. Experimental setup comprised of the standard "return to start" sequence, in the compression mode, with a distance of 50 mm as the target and "button" as the trigger type. An initial high-speed setting of 2 mm/s was used to prevent clogging of the needle tip. Once a proper flow was established, a lower speed setting of 0.6 mm/s was used and the crosslinker bath moved in a circular direction.

After extrusion, the produced bioabsorbable sutures were left to cure in the crosslinker solution for 15 min after which they were repeatedly washed, using five clean deionized water baths to remove any residual crosslinker from the bioabsorbable suture surface. Hereafter, the bioabsorbable sutures were placed on ointment tiles in a lamellar flow hood to dry until a constant diameter was achieved (±40 min).

Preparation of the bioabsorbable suture is based on the principle of physical crosslinking, that is, where an alginate-based polymer solution is extruded into a $BaCl_2$ crosslinker bath, the polymer solution will immediately solidify upon contact with the crosslinker to form a more rigid, insoluble polymer matrix. This phase change is the result of an ionic interaction between a cation of the crosslinker (Ba^{2+}) and two negatively charged carboxylate ions ($—COO^-$) of the alginate molecule, that bind the polymer chains together in an egg-box model fashion, that has been aptly described by Hu et al.[15] The rapid rate of crosslinking, associated with physical crosslinkers such as $BaCl_2$, as well as the circular motions performed during the crosslinking process, enables the formation of a long string-like material that resembles commercial sutures after drying.

2.3 | Coating of the bioabsorbable sutures with a lipid–drug layer

Various methods of drug loading were explored, including direct loading of the drug into the bioabsorbable suture matrix, soaking of the bioabsorbable suture and coating with several lipid–drug layers. A modified dip coating method, based on the work of Obermeier et al, was found to provide the most desirable drug loading and release properties and is described here.[16] The coating material was prepared by dissolving soy phosphatidyl choline (soy PDC) and dexamethasone (60:40) in 7.9 g ethanol to obtain a combined mass content of 5% (wt/wt). Bioabsorbable sutures were placed on the same ointment tiles, that were used during the drying process, and coated with the lipid-drug solution in a drop wise fashion. Coated bioabsorbable sutures were placed in a fume hood for rapid evaporation of ethanol and to improve adherence of the lipid–drug layer to the bioabsorbable suture surface. Optimal drug loading was achieved with a single drop coating round.

2.4 | Characterization and in vitro evaluation of the bioabsorbable sutures

2.4.1 | Mechanical properties

The functionality, applicability, and success of the newly developed bioabsorbable suture, hinges on its mechanical properties, which must

TABLE 2 The composition of bioabsorbable suture samples that were evaluated for mechanical performance

Formulation	Alginate (6% wt/vol)	Glycerol (4% vol/vol)	Pectin (0.1% wt/vol)	Gelatin (3% wt/vol)	Lipid-drug coating
A	+	−	−	−	−
B	+	−	+	−	−
C	+	−	−	+	−
D	+	+	−	−	−
E	+	+	+	+	−
F	+	+	+	+	+

comply with the United States Pharmacopeia (USP) guidelines for the minimum tensile strength of absorbable suture materials. Since the mechanical properties of a good suture material are multifaceted and require an intricate balance between strength and elasticity, we went through a lengthy process of evaluating the influence of different formulation components and ratios to finally identify the optimized bioabsorbable suture formulation. As explained previously and illustrated in the Supporting Information, alginate (6% wt/vol) was selected as base material and built upon to reach the desired suture-like properties. Glycerol was added as plasticizer to the carbohydrate-based formulation and the influence of increasing concentrations (0–12% vol/vol) on the stress–strain curves of the bioabsorbable sutures, studied. The influence of pectin (0–2% wt/vol) and gelatin (0–6% wt/vol) as reinforcing agents were also evaluated and significant improvements noted. To accurately evaluate the mechanical properties of the different bioabsorbable suture formulations, the diameter of each suture sample was first measured at three points along its length (in the middle and at each end) using a digital vernier calliper (Grip GV9371, Builders, SA) as described in the USP guidelines for suture diameter measurement. The tensile properties were measured using the Texture Analyser in the tensile mode, while fitted with the mini tensile grips (A/MTG, Stable Micro Systems, England). Bioabsorbable sutures samples were secured in the middle of the grips, with an active gauge length of 4 cm and the test performed at a constant rate of 80 mm/min, as specified by the USP standards for tensile testing.[17] To illustrate the improving mechanical properties of the bioabsorbable sutures with the addition of the selected formulation components in their optimized concentrations and ratios, the stress–strain curves of the formulations provided in Table 2, are discussed in detail. The influence of the lipid-drug coating of the mechanical performance of the bioabsorbable sutures, were equivalently evaluated.

Each formulation was evaluated in the straight ($n = 10$) and knot ($n = 10$) configuration, where a single overhand throw knot was placed in the centre of the bioabsorbable suture sample. The average was calculated and presented as the mean, ± standard error, for all 10 readings of each configuration. Load–displacement and stress–strain curves were generated, and the data used to calculate the tensile strength, elongation at break, Young's modulus, and toughness of each formulation. Using established principles, the slope of the stress–strain curve and the area under the curve (AUC), was used to respectively determine the Young's modulus and toughness. The tensile strength and elongation at break of the monofilament bioabsorbable sutures were computed using Equations (1) and (2).

$$\text{Tensile strength} = \frac{\text{load failure}}{\text{CSA}} \quad (1)$$

where load failure is the maximum load (N) at failure (i.e., where the bioabsorbable suture breaks) and CSA is the cross-sectional area (mm^2) of the bioabsorbable suture.

$$\text{Elongation at break} = \frac{l_1 - l_0}{l_0} x\,100 \quad (2)$$

where l_0 is the initial length of the bioabsorbable suture, and l_1 is the final length of the bioabsorbable suture.

Additionally, the influence of pectin on the extrudability of the bioabsorbable suture formulation through a 23G needle was evaluated by measuring the minimum force required to extrude each formulation through the needle into the crosslinker solution ($BaCl_2$, 2% wt/vol) using the Texture Analyser with the same settings that were used during bioabsorbable suture fabrication. This data provided insight into the ease of flow and resistance experienced with each formulation.

2.4.2 | Surface morphology analysis of the bioabsorbable sutures

The specific surface morphology of the bioabsorbable sutures were investigated before and after coating using a scanning electron microscope (Phenom™ Scanning Electron Microscope, FEI Company, OR, USA). Before analysis, bioabsorbable suture samples (approximately 1 cm in length) were mounted onto aluminium stubs, secured with carbon adhesive tape, and coated with carbon and palladium/gold in a 2:1 ratio.

2.4.3 | Molecular vibrational analysis of the bioabsorbable suture and materials

The spectral data for respective biopolymers, bioabsorbable sutures and the lipid-drug coated bioabsorbable sutures, were acquired to confirm the compatibility of the biopolymers,

the effective crosslinking of the bioabsorbable sutures and their successful coating with the lipid-drug layer. Absorption spectra were recorded from 4000 to 650 cm^{-1} on the Perkin-Elmer Spectrum 2000 FTIR spectrometer (PerkinElmer 100, Wales, UK).

2.4.4 | Powder X-ray diffraction analysis

The X-ray diffraction (XRD) spectra of the biopolymers, the bioabsorbable suture and the lipid-drug coated bioabsorbable suture were recorded on the MiniFlex 600 benchtop diffractometer (Rigaku, Japan). Under CuKα radiation continuous sample acquisition was carried out from 2° to 90°.

2.4.5 | Observation of thermal events in the bioabsorbable sutures

Selected thermal events were analyzed with differential scanning calorimetry (DSC; DSC 1, fitted with STARe [sensor] System, Mettler Toledo, Switzerland). Pre-weighed amounts of (3–10 mg) of the individual biopolymers and the uncoated and coated bioabsorbable sutures, were sealed in aluminium crucibles and heated at 5°C/min from 0 to 400°C under N_2 atmosphere.

2.4.6 | In vitro drug release studies

The amount of DEX released from the lipid-drug coated bioabsorbable sutures was measured by means of ultra-violet (UV) spectroscopy using the nanophotometer (Implen GmbH, München, Germany). The wavelength of maximum absorbance (λmax) for DEX in phosphate buffered saline (PBS, pH 7.4) was determined as $\lambda = 241$. A calibration curve for DEX was constructed by measuring the absorbance of standard solutions with known DEX concentrations. The linear regression equation of the calibration curve in this study is $y = 0.0575x - 0.0299$ ($R^2 = 0.9983$). To determine the drug release profile of DEX, three 2 cm segments of the coated bioabsorbable suture was prepared and placed in Eppendorf tubes containing 10 ml of PBS (pH 7.4). The samples were kept in a shaker incubator (Orbital shaker incubator, LM-530, Lasec Scientific equipment, Johannesburg, South Africa) rotating at 25 rpm at a temperature of 37°, to mimic the expected in vivo conditions. At predetermined time intervals (0.5, 1.5, 3, 6, 12, 24, 48, 72, 96, 120, 144 and 168 h), 2 ml was removed from each Eppendorf tube and replaced with fresh PBS to ensure that sink conditions where maintained. For each time point, the amount of drug released was calculated by measuring the absorbance of the solution at $\lambda = 241$ and substituting the value into the linear regression equation. To account for any random errors, the experiment was conducted in triplicate and the average results where further analyzed and graphically represented. The cumulative drug release was determined using Equation (3).

$$\text{Cumulative release}\,(\%) = \frac{C_t}{C_i} \times 100 \tag{3}$$

where C_t is the amount of DEX released at time t, and C_i is the amount of DEX loaded onto the bioabsorbable suture sample.

2.4.7 | In vitro swelling and degradation behavior of the bioabsorbable sutures

The ability of the uncoated and coated bioabsorbable sutures to absorb water was evaluated by incubation of pre-weighed samples in 10 ml of PBS (pH = 7.4) at 37°C. Samples were withdrawn from the PBS solution at frequent time points (10, 20, 30 and 50 min and 1, 2, 3, 4, 8, 12, 24 h) to determine the swelling rate and time point of equilibrium swelling. Filter paper was used to remove water that was retained on the surface of the samples, before weighing on a precision microbalance (A&D Instruments Limited, Oxfordshire, OX14 1DY, UK). The swelling ration (SR) was calculated using Equation (4):

$$\text{SR} = \frac{W_s - W_d}{W_d} \tag{4}$$

where W_s is the weight of the swollen sample and W_d the original weight of the dry sample.

The mechanical properties of the bioabsorbable sutures in their swollen state was evaluated after submersion of the filaments in PBS for 5 min, using the same methods described in section 2.4.1.

The degradation profiles of the coated and uncoated bioabsorbable sutures were evaluated in terms of weight loss over time. Pre-weighed samples were again incubated in 10 ml fresh PBS (pH = 7.4) at 37°C, rotating at 25 rpm. Samples were removed after 1, 2, 3 and 4 weeks of incubation, placed on absorbent filter paper and allowed to dry under lamellar flow in a fume hood. Once the samples were dry and achieved a constant diameter, they were accurately weighed on a precision microbalance and the percentage weight loss (i.e., degradation) calculated using Equation (5).

$$\text{Percentage degradation} = \frac{W_o - W_t}{W_i} \times 100 \tag{5}$$

where W_o is the original, starting weight of the sample and W_t is the weight at time t, after incubation in PBS. Results were expressed as mean ± standard deviation of three analysis performed. The appearance of the bioabsorbable sutures during the degradation process was studied by imaging the dried, weighed samples with a scanning electron microscope (Phenom™ Scanning Electron Microscope, FEI Company, OR, USA).

2.4.8 | In vitro hemocompatibility of the bioabsorbable sutures

The hemocompatibility of the bioabsorbable sutures was evaluated by means of a haemolysis assay, as previously described by Sunitha et al, as well as a platelet activation assay, detailed by Jung et al.[18,19] The haemolysis assay was executed as per ISO 10993 protocols, with sodium citrate (3.8% wt/vol) stabilized blood (5.4 ml), obtained from a healthy human volunteer. Before starting the assay, extracts of the uncoated and coated bioabsorbable sutures were prepared by incubating segments of the bioabsorbable sutures (5 cm/ml) in freshly prepared phosphate buffered saline (PBS, pH = 7.4), for 24 h at 37°C. At the time of the assay, the whole blood was centrifuged at 3000 rpm for 15 min and the erythrocyte pellet washed twice with PBS. The erythrocytes were diluted with PBS to achieve an 8% (vol/vol) concentration and 1 ml aliquots transferred into 2 ml Eppendorf tubes. Extracts of the uncoated and coated bioabsorbable sutures, as well as a solution of the drug (50 ug/ml), were added to the erythrocyte suspensions (0.5 ml), which were then incubated for 1 h at 37°C, 25 rpm. Post incubation, the erythrocyte suspensions were centrifuged (3000 rpm) for 15 min and the absorbance of the supernatants measured at 540 nm using a multiplate reader (VICTOR™ X Multilabel Plate Reader, Perkin Elmer, SA). Triton X-100 (1% vol/vol) was used as positive control and PBS as negative control. The application of Equation (6) yielded the average percentage hemolysis for assays performed in triplicate:

$$\%\text{Haemolysis} = \frac{OD_s - OD_n}{OD_p - OD_n} \times 100 \quad (6)$$

where OD_s, OD_n, and OD_p represent the absorption readings of the sample, negative control and positive control, respectively.

Platelet activation was evaluated microscopically, by studying the change in platelet shape as a function of incubation with bioabsorbable suture extracts. Briefly, whole blood was centrifuged (1200 rpm) for 15 min to obtain platelet rich plasma (PRP) and the platelets (406 x 10^4 platelets/ml) seeded into a 48 well plate. Extracts of the uncoated and coated bioabsorbable sutures (5 cm/ml) were prepared by incubation in PBS for 24 h at 37°C and 0.1 ml of each extract added to the wells in triplicate. Collagen (100 ug/ml) served as positive control and PBS and negative control. After static incubation for 1 h at r.t., the treated wells were visualized with an Olympus light microscope (Olympus CKS microscope, Olympus, Japan) and the morphology of the platelets studied.

2.4.9 | In vitro cytocompatibility of the bioabsorbable sutures

The biocompatibility of the bioabsorbable sutures were assessed using human embryonic kidney (HEK 293) cells, due to availability and the human origin of the cell line. Cells were maintained in Dulbecco's minimal essential medium (DMEM), supplemented with 10% fetal calf serum (FCS) and antibiotics (100 IU/ml penicillin and 100 IU/ml streptomycin). The in vitro cytotoxicity assay was performed as outlined by ISO 10993-5, using the indirect extract method. Extracts were prepared by incubating the uncoated and coated bioabsorbable sutures (5 cm/ml) in fresh culture media for 5 days. High extract concentrations were used in order to exaggerate the clinical use conditions and determine any potential toxicological hazard. HEK 293 cells were seeded in 96-well cell culture plates (3 x 10^3 cells/well) and incubated for 24 h. The culture media of some wells were then removed and replaced with extract medium, while other wells were treated with the drug solution, positive control (5-fluorouracil, 1% wt/vol) or negative control (fresh medium). All treatments were performed in triplicate across a concentration range of 5, 2.5 and 1.25 cm/ml for the bioabsorbable suture extracts and 0.5, 0.25 and 0.125 mg/ml, for the drug solutions, in correspondence with the amount of drug loaded on the coated bioabsorbable sutures. The cells were subjected to incubation in a humidified chamber at 37°C and 5% CO_2 for 24 and 48 h. At the end of the incubation period, the cell viability was determined by XTT assay according to the standard protocol. Briefly, 100 ul of the electron coupling reagent (ECR) was added to 5 ml of the XTT labeling reagent and 50 ul of the XTT mixture immediately added to each well (final concentration, 0.3 mg/ml) followed by incubation for 4 h. Absorption readings were recorded with a multiplate reader (VICTOR™ X Multilabel Plate Reader, Perkin Elmer, SA) at 450 nm, with 650 nm as reference wavelength. Equation (7) was applied to compute the percentage cell viability:

$$\text{Cell viability}\,(\%) = \frac{Abs_s}{Abs_c} \times 100 \quad (7)$$

2.5 | Statistical analysis

All calculated data are presented as mean ± standard deviation, with a minimum of three samples ($N = 3$) evaluated. To account for variation between data sets the Student's t-tests was applied and the data in figures are demarcated by (*) for $p < .05$ and (**) for $p < .01$.

3 | RESULTS AND DISCUSSION

3.1 | Characterization and in vitro evaluation of the bioabsorbable sutures

3.1.1 | Analysis of the mechanical properties of the bioabsorbable sutures

The most defining property of any suture material is its mechanical performance. A suture material that is not robust enough to withstand the pressures of handling during surgery, or strong enough to approximate wound edges, will not be able to perform its basic function of wound closure. Yet, a suture material that is too rigid and strong will

TABLE 3 Mechanical properties of different bioabsorbable suture formulations

Formulation	Load failure (N)	Tensile strength (N/mm^2)	Elongation at break (%)	Young's modulus (MPa)	Toughness (J mm^{-3})
Straight configuration					
A. Alg	2.07 ± 0.9	183.12 ± 0.9	13.77 ± 0.4	0.85 ± 0.3	7.12 ± 0.6
B. Alg-Pec	2.97 ± 0.7	591.66 ± 0.7	14.60 ± 0.3	1.67 ± 0.4	16.82 ± 0.8
C. Alg-Gel	3.44 ± 0.6	304.07 ± 0.6	20.52 ± 0.6	1.33 ± 0.7	9.43 ± 0.7
D. Alg-Gly	3.23 ± 0.7	286.39 ± 0.7	19.64 ± 0.6	1.27 ± 0.5	18.52 ± 0.7
E. Alg-Gly-Pec-Gel	4.08 ± 0.4	360.39 ± 0.4	18.55 ± 0.9	2.04 ± 0.4	10.52 ± 0.6
F. Coated	4.14 ± 0.7	366.23 ± 0.7	18.57 ± 0.5	2.06 ± 0.5	10.83 ± 0.5
Knot configuration					
A. Alg	1.3 ± 0.6	116.18 ± 0.6	4.47 ± 0.5	1.31 ± 0.7	0.91 ± 0.4
B. Alg-Pec	2.02 ± 0.5	402.66 ± 0.5	7.36 ± 0.3	1.52 ± 0.6	1.44 ± 0.6
C. Alg-Gel	1.92 ± 0.7	170.03 ± 0.7	10.06 ± 0.8	1.16 ± 0.6	1.99 ± 0.5
D. Alg-Gly	2.13 ± 0.7	188.33 ± 0.7	9.01 ± 0.5	1.19 ± 0.5	2.55 ± 0.9
E. Alg-Gly-Pec-Gel	2.44 ± 0.3	216.09 ± 0.3	9.47 ± 0.4	1.51 ± 0.4	2.59 ± 0.3
F. Coated	2.59 ± 0.4	229.27 ± 0.4	10.26 ± 0.7	1.56 ± 0.3	2.78 ± 0.7

not have sufficient elasticity to tie proper knots or to expand with the wound during swelling, which could in turn also deter its performance and ability to facilitate wound healing.[20] A fine balance must, therefore, be struck between the tensile strength and elongation at break of suture materials. Hence, these mechanical properties were our main focus during the development of the novel bioabsorbable suture. Various biopolymers, with distinct characteristics that make them particularly suitable for bioabsorbable suture material development, were investigated at different concentrations and ratios to obtain a final bioabsorbable suture formulation that will comply with the United States Pharmacopeia (USP) guidelines for suture material strength.[17] Table 3 provides the load failure (N), tensile strength (N/mm^2), elongation at break (%), young's modulus (MPa) and toughness (J mm^{-3}) of bioabsorbable suture formulations with the optimized component concentrations and clearly indicates the improvement in mechanical properties that was achieved with the addition of each selected biopolymer at its ideal concentration.

The initial, pure alginate formulation showed immense promise for application as a bioabsorbable suture with good handling characteristics and a low diameter (0.10 mm ± 0.01) that corresponded with a 6–0 suture size. Yet, the mechanical properties had to be improved in order to yield a functional and clinically acceptable bioabsorbable suture. With the addition of pectin, the behavior of the biopolymer solution instantaneously changed—it became less viscous and flowed out of the needle tip with greater ease than the pure alginate formulation. The resulting bioabsorbable sutures after drying depicted better morphology and resembled straighter, thinner and more suture-like characteristics. Texture Analyzer data indicated that the combined polymer solution required less force (95 *N* compared to 107 *N*) to be extruded through a 23G needle into the crosslinker solution (see Figure 1F). This can be ascribed to the synergistic behavior of alginate and pectin which has been shown to arrange in unique parallel two-fold crystalline arrays that present in the form of rigid ribbons according to Thom et al.[21] The alginate–pectin hydrogel, therefore, has a more linear arrangement of polymer chains that flow with greater ease and provides less resistance during extrusion, which can also be ascribed to the shear thinning behavior of the biopolymer solution.

The synergistic behavior of alginate and pectin can also be credited for the lower diameter of alginate–pectin bioabsorbable sutures which displayed an average size of 0.08 mm compared to the 0.10 mm of pure alginate bioabsorbable sutures. This result ties in well with previous studies wherein Bierhalz et al, as well as Lambrech et al, found that the addition of pectin to an alginate network results in a decrease in diameter of the fabricated fiber or film. They ascribed this change in diameter to increased molecular interactions with the addition of pectin, that results in a change in microstructure (more compact molecular packing) with smaller pore sizes and greater network density.[22,23] Pectin also improved the mechanical properties of the bioabsorbable sutures by considerably increasing the load failure and tensile strength, in both the straight and knotted configuration, while slightly increasing the elongation at break, as can be seen in Table 3 and Figure 1. The toughness of the bioabsorbable sutures were also substantially higher after the addition of pectin at the selected concentration (0.1% wt/vol) which attests to its ability to increase the tensile strength of the bioabsorbable suture, without causing a detrimental decrease in elasticity as was observed with other, more crystalline biopolymers. It should be noted that the addition of increasing concentrations of pectin, however, resulted in a decrease in the load failure (N), tensile strength (N/mm^2) and elongation at break (%) of the bioabsorbable sutures, as shown in Figure 2. This can be ascribed to the higher crystallinity of the formulations with higher pectin concentrations and points to an optimal alginate–pectin ratio where maximum synergy is observed, as discussed by Gohil and Walkenström.[24,25] In summary, low and optimal concentrations of pectin improves the mechanical performance of the alginate-

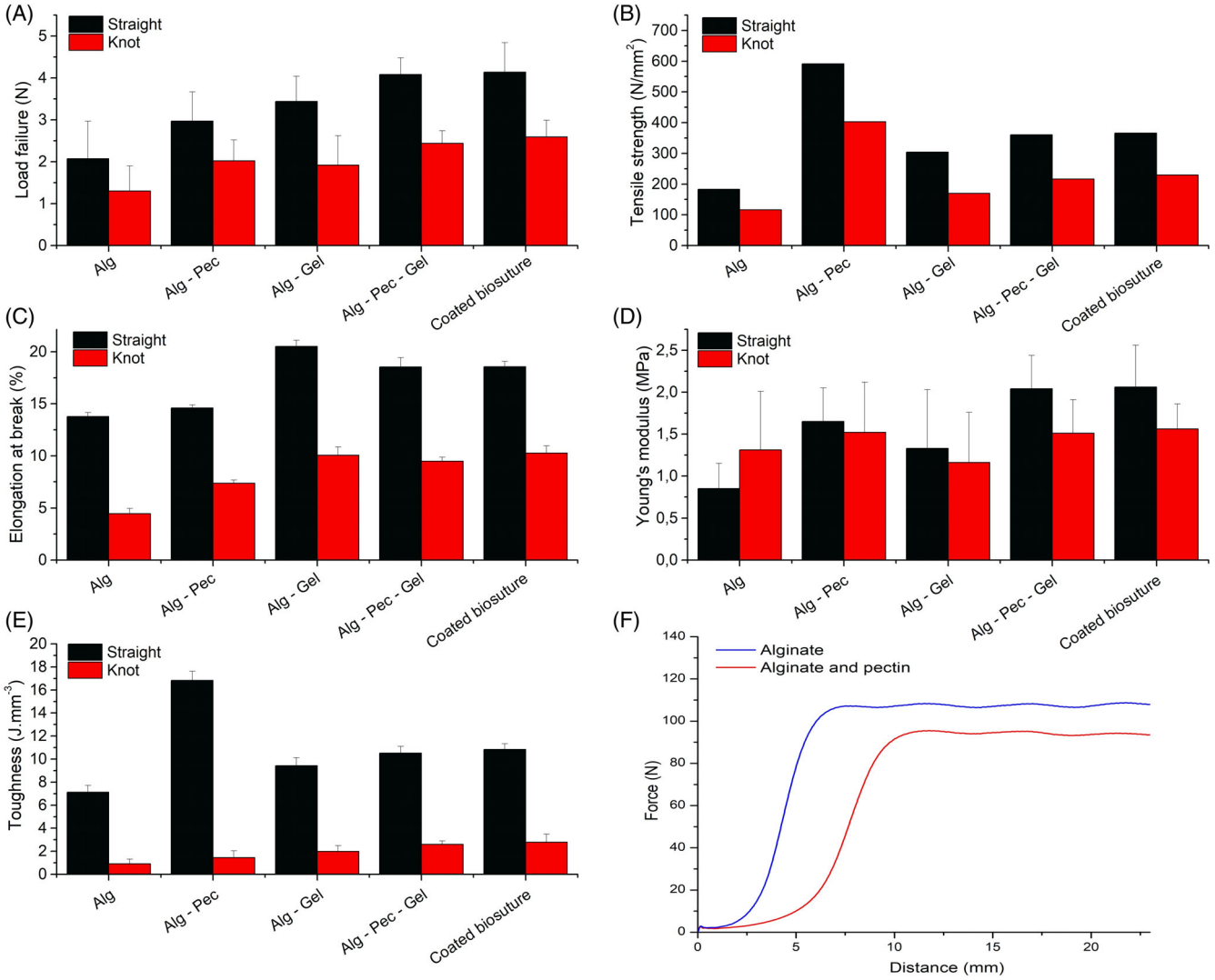

FIGURE 1 (A) Load failure, (B) tensile testing results, (C) elongation at break, (D) Young's modulus, and (E) toughness of different biopolymeric suture formulations in the straight and knot configuration. (F) The force required to extrude alginate (blue) and alginate–pectin (red) solutions through a 23G needle into a crosslinker solution. *Biosuture = bioabsorbable suture

based bioabsorbable suture formulation, while higher concentrations diminish their strength.

Gelatin, on the other hand, also increased the load failure and tensile strength of the bioabsorbable sutures, while profoundly increasing the elongation at break and elasticity of the bioabsorbable sutures. Other authors, such as Taira et al, also found that gelatin can greatly improve the elasticity of polymeric systems and ascribed this to the hygroscopic nature of the biopolymer that draws additional water molecules to the system, which in turn exerts a plasticizing effect.[26] Wang et al, noted that the increase in plasticity caused by gelatin is concentration dependent and will lead to a decrease in tensile properties and elasticity once a critical concentration is exceeded.[27] Similar results were found in the current study (Table 4), where increasing concentrations of gelatin, gradually improved the mechanical properties of the bioabsorbable sutures, until it reached a plateau around 3% wt/vol, after which the mechanical properties of the bioabsorbable sutures suddenly plummeted. In the current investigation, 3% (wt/vol) was selected as the optimal gelatin concentration due to a good balance between strength and elasticity found at this concentration.

Plasticizers are a critical part of most natural polymer-based formulations as they dramatically improve the flexibility and elasticity of the systems. Plasticizers are known to decrease the straight tensile strength of suture materials, while increasing their elongation at break.[28] A higher elongation at break usually improves the handling properties, knot-tying abilities, and knot tensile strength of suture materials, and could therefore, improve the overall performance of the bioabsorbable sutures. After experimentation with different plasticizers, glycerol was identified as the plasticizer of choice due to its inherent biocompatibility, water-solubility, excellent plasticizing effect and superior ability to integrate with, and remain within the biopolymer system. Contrary to what was expected, the addition of glycerol at concentrations 2%–4% vol/vol to the biopolymer system did not

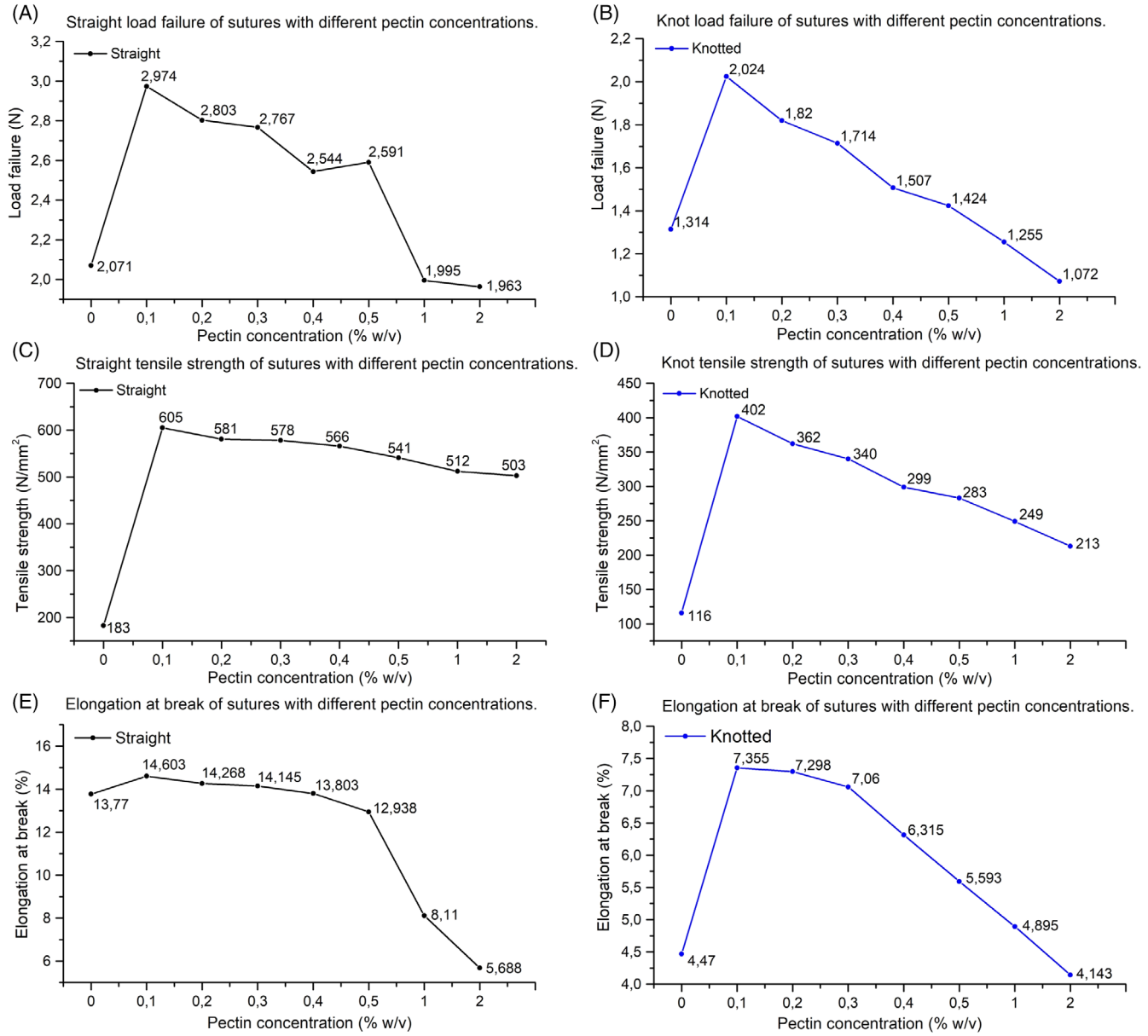

FIGURE 2 Load failure (N), tensile strength (N/mm^2) and elongation at break (%) of bioabsorbable suture samples containing different concentrations of pectin in the straight (A, C and E) and knot (B, D and F) configuration

cause a decrease in strength, but resulted in an overall increase in load failure, tensile strength, elongation at break, and toughness, compared to alginate alone (Table 3). This was previously observed by Gao et al, who proved, by means of X-ray diffraction analyses, that glycerol increases alginate chain mobility, while also promoting crystallization of polymer through structural reorganization.[29] Higher concentrations of glycerol, however, resulted in the predicted decrease in load failure and tensile strength and increase in elongation at break, pointing to a concentration dependant effect, similar to what was observed with pectin and gelatin. The most profound impact of glycerol of the performance of the bioabsorbable sutures, was seen in the knotted configuration. The sutures were noticeably more manageable and could effectively tie and secure a knot, as signified by the bimodal structure of the stress–strain curve in the knotted configuration. The first mode signifies the load carried while the knot is tightening, while the second mode signifies the load withstood after the knot is secured. As shown in Figure 3, the stress–strain curve of the bioabsorbable sutures consisting of only alginate, does not display the characteristic bimodal shape, signifying that the bioabsorbable suture broke before the knot was secured (Figure 3).

The combination of alginate, pectin, gelatin, and glycerol in their optimized concentrations, resulted in bioabsorbable sutures with even greater mechanical properties than the combination of only two of the components. The knot load failure of the final bioabsorbable suture formulation (2.44 *N*), far exceeded the minimum value required by the USP (1.76 *N*), suggesting that the newly developed

TABLE 4 Variation in the mechanical properties of bioabsorbable sutures with increasing gelatin concentrations (% wt/vol) in the straight and knotted configuration

Alginate content (% wt/vol)	Gelatin content (% wt/vol)	Load failure (N)	Tensile strength (N/mm^2)	Elongation at break (%)
Straight configuration				
6	0	2.071 ± 0.91	183.116 ± 0.91	13.77 ± 0.43
6	0.75	2.115 ± 0.72	187.007 ± 0.72	14.26 ± 1.04
6	1.5	2.253 ± 0.81	199.208 ± 0.81	17.31 ± 0.72
6	3	3.439 ± 0.67	304.074 ± 0.67	20.52 ± 0.64
6	6	2.721 ± 0.77	240.589 ± 0.77	15.19 ± 0.97
Knotted configuration				
6	0	1.314 ± 0.62	116.183 ± 0.62	4.47 ± 0.51
6	0.75	1.359 ± 0.81	120.161 ± 0.81	7.05 ± 0.63
6	1.5	1.439 ± 0.89	127.235 ± 0.89	9.19 ± 0.78
6	3	1.923 ± 0.78	170.031 ± 0.78	10.06 ± 0.85
6	6	1.541 ± 0.91	136.254 ± 0.91	7.79 ± 0.65

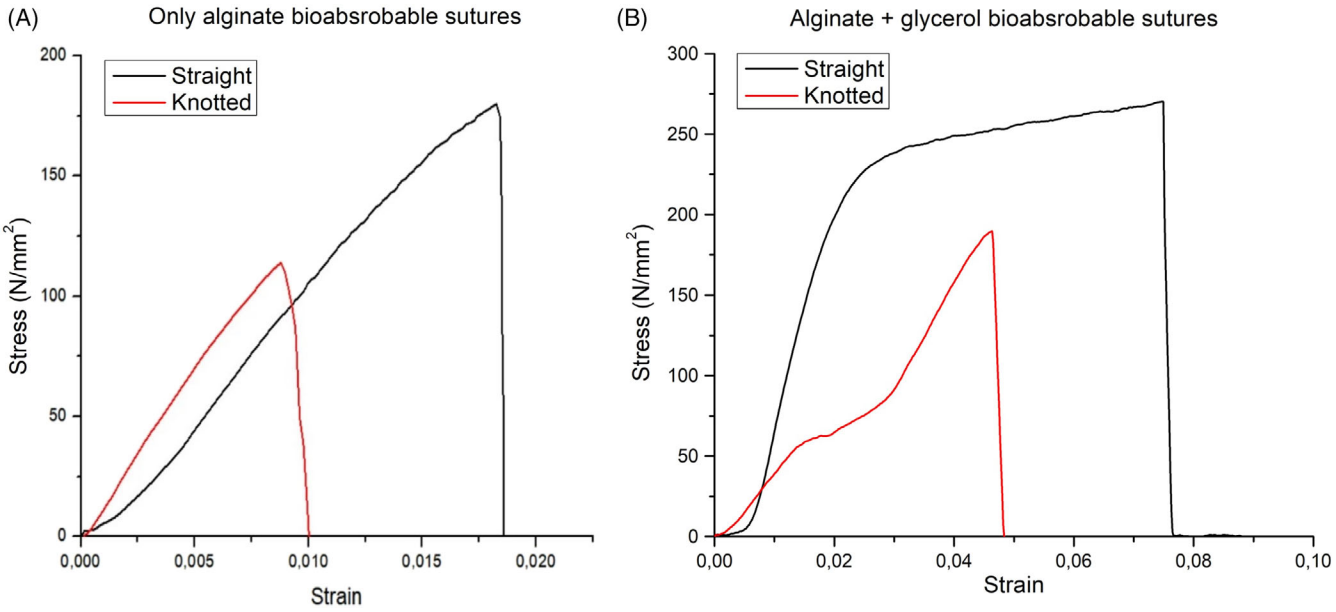

FIGURE 3 Stress strain curves of bioabsorbable sutures containing only alginate (A) and containing alginate and glycerol (B)

bioabsorbable sutures will be clinically effective and able to properly approximate wound edges.[17] Interestingly, the coated bioabsorbable sutures displayed slightly better mechanical properties than the uncoated bioabsorbable sutures with a final knot load failure of 2.59 *N*. The elongation at break of the uncoated and coated bioabsorbable sutures were more or less the same in the straight configuration, but slightly higher for the coated bioabsorbable sutures in the knotted configuration (9.47% compared to 10.26%). This can be ascribed to the lubricating effect of the lipid-drug layer that allows the coated bioabsorbable sutures to tie tighter knots and elongate for longer. Additionally, the coating process could have led to slight dehydration of the bioabsorbable suture system, as a result of immersion in an organic solvent, which would have led to a more compact network with greater tensile strength.[30]

As can be seen in Figure 2, the stress–strain curves of the uncoated and coated bioabsorbable sutures are very similar, with the coated bioabsorbable sutures reaching slightly higher tensile stress before fracturing. The Young's modulus of the bioabsorbable sutures is more or less the same before and after coating, while the toughness slightly increased (see Table 2). This suggests that the stiffness of the material was not drastically altered by the coating process, but that the coated bioabsorbable suture is able to undergo a greater amount of plastic deformation and absorb more energy than the uncoated bioabsorbable suture before breaking. This is a highly desirable quality in any suture material and suggests that the bioabsorbable suture will tend to bend rather than break during handling and knot tying. The stress–strain curves of the bioabsorbable sutures in the knotted configuration, display the desirable bimodal shape where the first mode

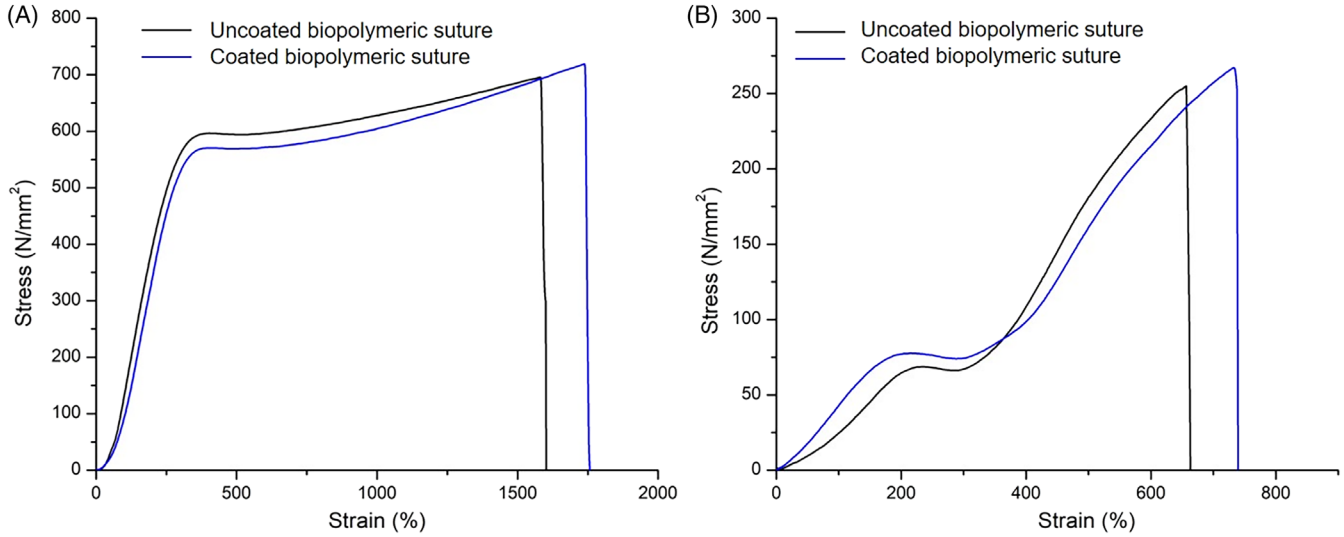

FIGURE 4 Stress–strain curves of the uncoated and coated bioabsorbable sutures in the (A) straight configuration and (B) knotted configuration

TABLE 5 Mechanical properties of the novel bioabsorbable suture compared to that of standard commercial sutures, that is, 6/0 Prolene® polypropylene sutures and 6/0 Surgicryl® 910 polyglactine sutures, in the knotted configuration

Suture	Load failure (N)	Tensile strength (N/mm^2)	Elongation at break (%)	Young's modulus (MPa)	Toughness ($J\ mm^{-3}$)
Knotted configuration					
Uncoated alg-pec-gel-gly	2.44 ± 0.3	216.09 ± 0.3	9.47 ± 0.4	1.51 ± 0.4	2.59 ± 0.3
Coated alg-pec-gel-gly	2.59 ± 0.4	229.27 ± 0.4	10.26 ± 0.7	1.56 ± 0.3	2.78 ± 2.8
Prolene® polypropylene	2.11 ± 0.3	186.56 ± 0.3	14.24 ± 0.6	1.05 ± 0.5	0.37 ± 2.2
Surgicryl® Polyglactin	2.82 ± 0.5	249.61 ± 0.5	10.05 ± 0.4	1.64 ± 0.5	2.87 ± 2.6

represents the tightening of the knot, and the second mode reflects the inherent properties of the material. It is widely accepted that the knot is the weakest point of a suture and the primary position where the material will fracture, and the same observation was made in the current study. Yet, as can be deduced from Figure 2B, the bioabsorbable sutures were able to withstand an impressive amount of stress and strain after tightening of the knot, before finally rupturing at the knot site (Figure 4).

Furthermore, the knot tensile strength of the bioabsorbable sutures produced in this study, compared exceptionally well with standard synthetic sutures of the same size (Table 5), which confirms the suitability of the bioabsorbable sutures for clinical use. The Prolene® sutures, which consist of polypropylene, were considerably more elastic than the bioabsorbable and Surgicryl®, a likely result of the inherent flexible nature of the material. This provided the Prolene® sutures with a higher elongation at break, but subsequently also a lower tensile strength, young's modulus, and toughness. The Surgicryl® Polyglactin sutures displayed very similar, albeit slightly higher load failure and tensile strength values, to the novel bioabsorbable sutures. This is a noteworthy accomplishment on the part of the bioabsorbable sutures, considering their monofilament structure compared to the braided, multifilament nature of the Surgicryl® sutures, which provides it with additional strength.

3.1.2 | Analysis of the surface morphology of the bioabsorbable sutures with SEM

SEM images (Figure 5) revealed a smooth, uniform bioabsorbable suture surface that should easily glide through tissues without causing significant damage. The uniform appearance of the bioabsorbable suture also confirms the compatibility and good distribution of the biopolymers that make up the material. The long fiber-like lines on the bioabsorbable suture surface can be attributed to the extrusion process during manufacturing and can also be a consequence of the long polymeric chains of alginate and pectin that form during crosslinking. The average diameter of several bioabsorbable suture samples ($n = 10$) was 115 μm, which corresponds with a 6–0 suture size, according to the USP monograph for absorbable surgical sutures. Figure 5B shows the coated bioabsorbable suture, which unfortunately cracked under the focussed electron beam of the microscope, but still confirms the successful coating of the bioabsorbable suture.

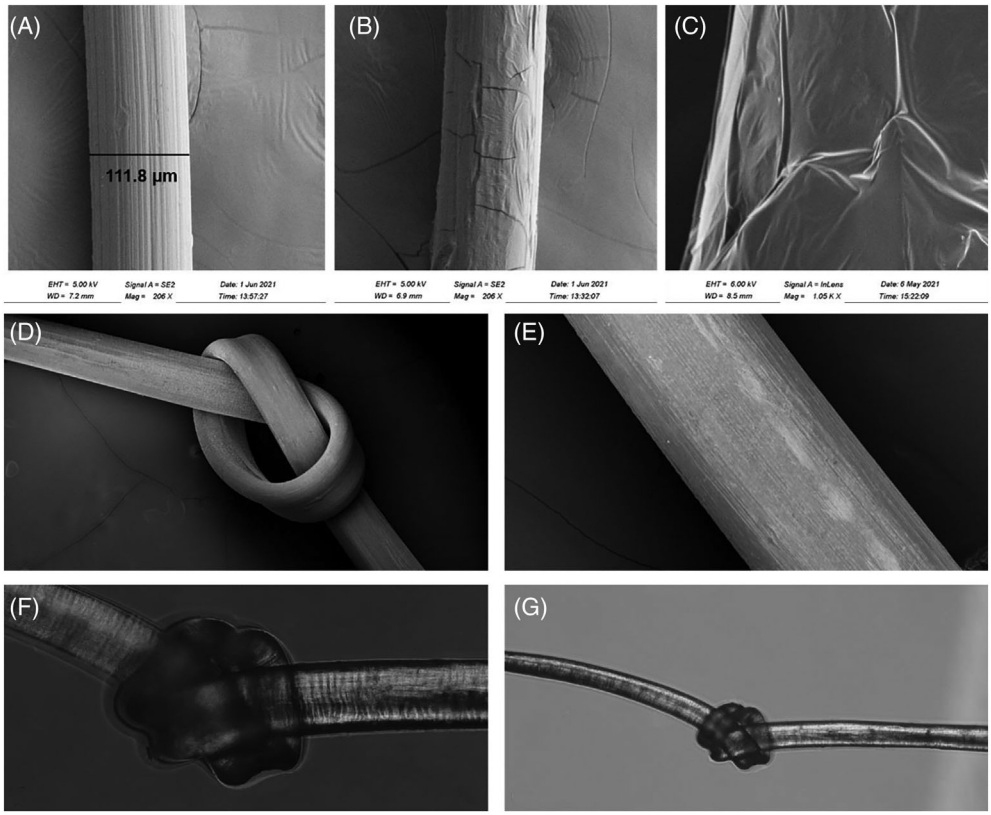

FIGURE 5 SEM images of the uncoated bioabsorbable suture (A) and coated bioabsorbable suture (B). Image (C) provides an enlarged (1.05 K magnification) image of the coated bioabsorbable suture without damage by the electron beam. Image (D) and (E) show in lens SEM images of the bioabsorbable suture in the straight and knotted configuration, respectively. Light microscope images (F) and (G) show the morphology of tightened knots made with bioabsorbable sutures

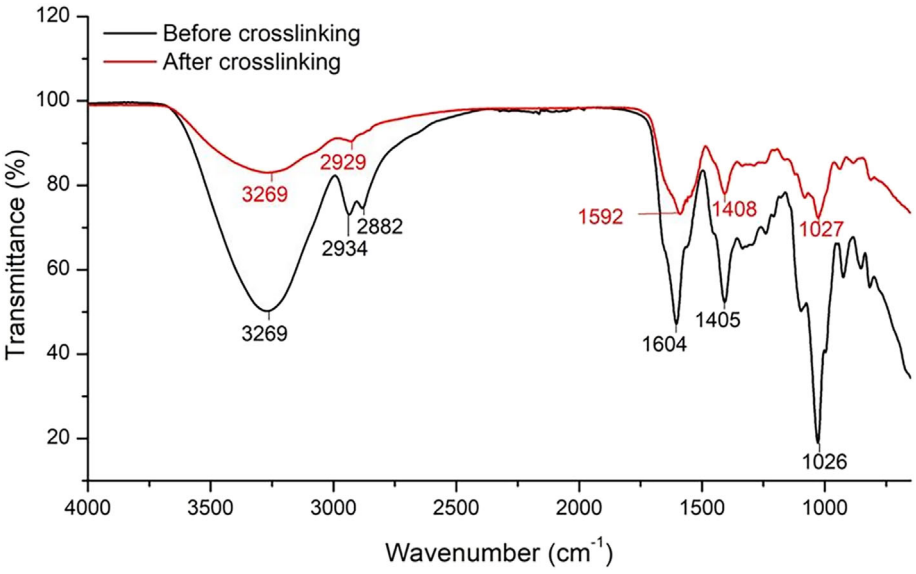

FIGURE 6 FTIR spectra of the bioabsorbable suture before (black) and after crosslinking (red) with $BaCl_2$

The lipid-drug coating looks like a silk draping that covers the bioabsorbable suture surface in a dramatic fashion. The fact that the coating remained on the bioabsorbable suture even after extensive handling and sample preparation, points to a good affinity of the coating material for the bioabsorbable suture surface and suggests that it will also remain on the bioabsorbable suture during suturing, which has previously been seen in similar coatings.[31] The SEM images also confirmed the good elasticity of the bioabsorbable sutures and their ability to tie knots (Figure 5E–G) without any sign of fracturing or breaking at the bends where the strain is at its highest.

3.1.3 | Determination of the molecular vibrational transitions of the bioabsorbable sutures using FTIR

The FTIR spectra of the individual components corresponded well with literature and can be found in the Supporting Information. The IR spectrum of the bioabsorbable suture (Figure 6) closely resembles the spectrum of the main component, that is, sodium alginate, with clear contributions from the second most abundant component, that is, glycerol. The presence of the other two biopolymers, that is, pectin and gelatin, is less prominent but can safely be deducted. These points

to good compatibility and effective incorporation of the low concentration polymers into the alginate matrix. The broad band around 3269 cm^{-1} was observed in the IR spectra of all the pristine polymers, but its intensity is greatly increased in the combined bioabsorbable suture formulation spectrum. This can be due to the combined contribution of all the hydroxyl groups in the various biopolymers which will increase the absorption in this region. This peak, even though broad, is narrower than in the case of the pristine polymers and resembles the deep absorption band of glycerol in this region, pointing toward its presence in the formulation. The peak also shifted from 3259 cm^{-1} (where it was observed in the alginate spectrum, as shown in Supporting Information) to 3269 cm^{-1}, which suggests that hydrogen bonds have formed between the different polymers and confirms their compatibility.

The weak peak at ~2900 cm^{-1}, was observed for all of the individual components and were ascribed to the stretching vibrations of the C—H groups of the polymers. In the bioabsorbable suture spectrum, however, the peak is bimodal which reveals both the symmetric and asymmetric stretching vibrations of the C—H groups, and confirms the presence of glycerol, which displayed a similar small bimodal peak in this region. In the region of 1550–1200 cm^{-1}, significant overlapping of absorption bands occurs, making the assignment of individual peaks more difficult. The two peaks at 1604 and 1405 cm^{-1} can be ascribed to the symmetric and asymmetric stretching vibrations of the —COO groups found in alginate. Yet, the 1604 cm^{-1} peak has a shoulder at 1560 cm^{-1} which can be ascribed to the free carboxylate groups of pectin. The strong peak at 1026 cm^{-1} can be ascribed to the C—C and C—O stretching vibrations of the pyranosyl ring which is found in both alginate and pectin. The weak peaks observed in the region 1330–1080 cm^{-1} could be representative of amide III–VI but is less clear due to interference and overlapping of the carbohydrate functional groups in the same region.

Upon comparison of the bioabsorbable suture formulation before and after crosslinking, it is clear that some change did occur on a molecular level during the crosslinking process. The most significant difference between the two spectra can be seen at the strong absorption bands that represent the —COO^- groups, which have shifted from 1604 to 1595 cm^{-1} and from 1405 to 1408 cm^{-1}, while broadening and lowering their intensity (outlined in Figure 4). This undoubtedly indicates a strong interaction between Ba^{2+} and the —CO of the carboxyl group in the polymer chains and confirms crosslinking of the bioabsorbable suture. Similar results were found by Awasthi et al, after they crosslinked an alginate–pectin network with Ca^{2+} for the sustained release of repaglinide.[32] Yet, there is no indication of the presence of Ba-Cl in the IR spectrum (which would have revealed a characteristic peak around 1635 cm^{-1}) and confirms that the washing process was effective in removing any excess barium chloride from the bioabsorbable suture surface.[33]

The IR spectra of the lipid-drug coating (shown in Figure 5) displays three very sharp peaks in the 3000–2800 cm^{-1} region (outlined in blue), which is characteristic of soy phosphatidyl choline and can be ascribed to the different C—H stretching vibrations of the molecule. These absorption bands also overlap with the stretching vibrations of the methyl groups in DEX, which could account for the high intensity of the peaks. The other three sharp peaks, found at 1742, 1665 and 1622 cm^{-1}, (circled in green) are characteristic of DEX and can be ascribed to the νC═O (aliphatic-C20), νC═O (cyclic [conjugated] C3), and νC═C (cyclic) of the drug molecule, while absorption at 1242 cm^{-1} (circled in red) is due to the stretching vibrations of the C—F bonds in dexamethasone. The IR spectrum of the coated bioabsorbable suture resembled that of the uncoated bioabsorbable suture's spectrum but with some additional absorption bands that confirm effective coating of the bioabsorbable sutures with the lipid-drug layer. Similar to the spectrum of the coating material, three sharp peaks can be observed in the 3000–2800 cm^{-1} region (outlined in blue), which were absent in the uncoated bioabsorbable suture spectrum. These peaks have not shifted significantly, even though their intensity slightly decreased (presumably because of the small quantity present on the suture surface), indicating no unwanted interaction between the coating material and the bioabsorbable suture and confirming that DEX should maintain its bioactivity. The sharp peak that can be observed at 1663 cm^{-1} (circled in green), as well as the important C—F indicating peak at 1242 cm^{-1} (circled in red), are characteristic of DEX and is indicative of the drug coated on the surface of the bioabsorbable suture (Figure 7).

The XRD spectra of the pristine biopolymers (see Supporting Information) were first analyzed and then compared to that of the bioabsorbable suture spectra. The diffraction pattern of sodium alginate revealed a semi-crystalline structure with two peaks at 2θ equals to 22.1° and 38.4°. The diffraction pattern of pectin, on the other hand, contained mostly sharp, narrow peaks that clearly pointed to a more crystalline nature. Gelatin, in turn, displayed a highly amorphous diffraction pattern with a single, slightly pronounced peak at 2θ equals to 21.9°. After combining the semi-crystalline alginate, with the crystalline pectin and more amorphous gelatin, the produced bioabsorbable suture displayed an amorphous diffraction pattern (Figure 8). Similar to the FTIR spectra, the diffraction pattern mostly resembled that of the main component, that is, alginate and displayed two peaks at 2θ equals to 25.4° and 40.1°.

The diffraction pattern of the coated bioabsorbable suture correlates well with that of the uncoated bioabsorbable suture except for sharp peaks at 2.5° and 15.3°, respectively. These fairly crystalline peaks are characteristic of DEX, and is further indicative of the presence of the drug in the coated bioabsorbable suture. Soy phosphatidyl choline is amorphous in nature and its contributing peaks is probably masked by that of the semi-crystalline bioabsorbable suture.

3.1.4 | Analysis of the thermal properties of the bioabsorbable sutures using DSC

The DSC results of the bioabsorbable suture revealed only two thermodynamic events (see Figure 9). The first is an endotherm at 50–150°C and represents the evaporation of water from the sample. No melting events were observed in the thermogram and the only other thermal event for the bioabsorbable suture is an exotherm around 222°C,

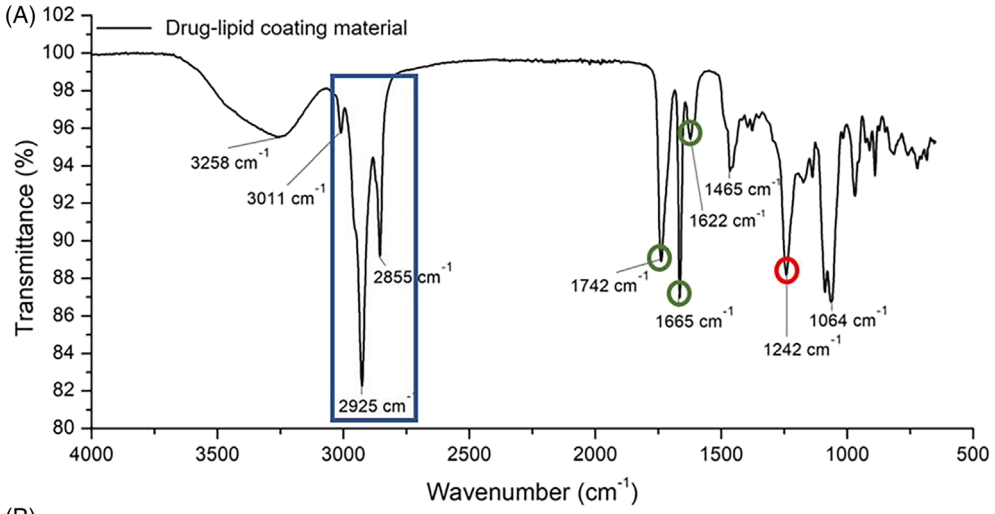

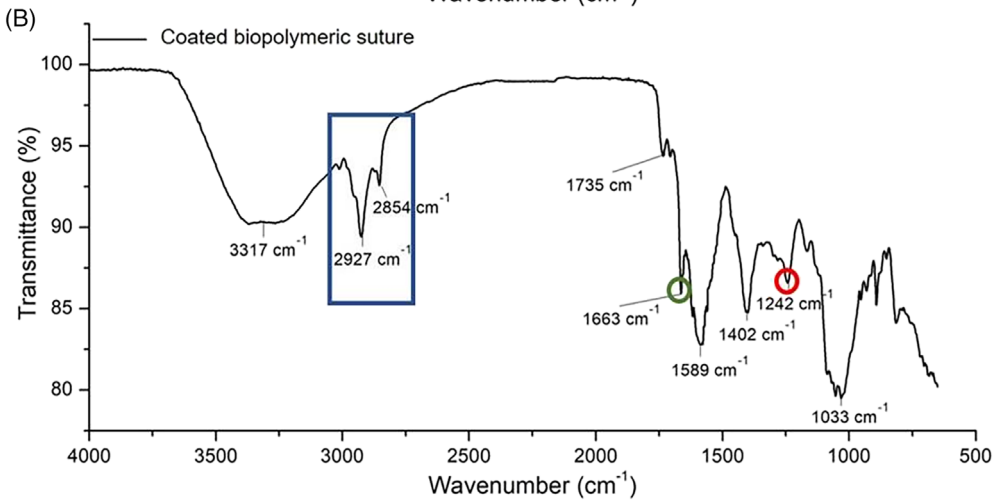

FIGURE 7 (A) FTIR spectra of the lipid-drug coating (consisting of soy phosphatidyl choline and dexamethasone) and (B) of the bioabsorbable suture coated with the lipid-drug coating

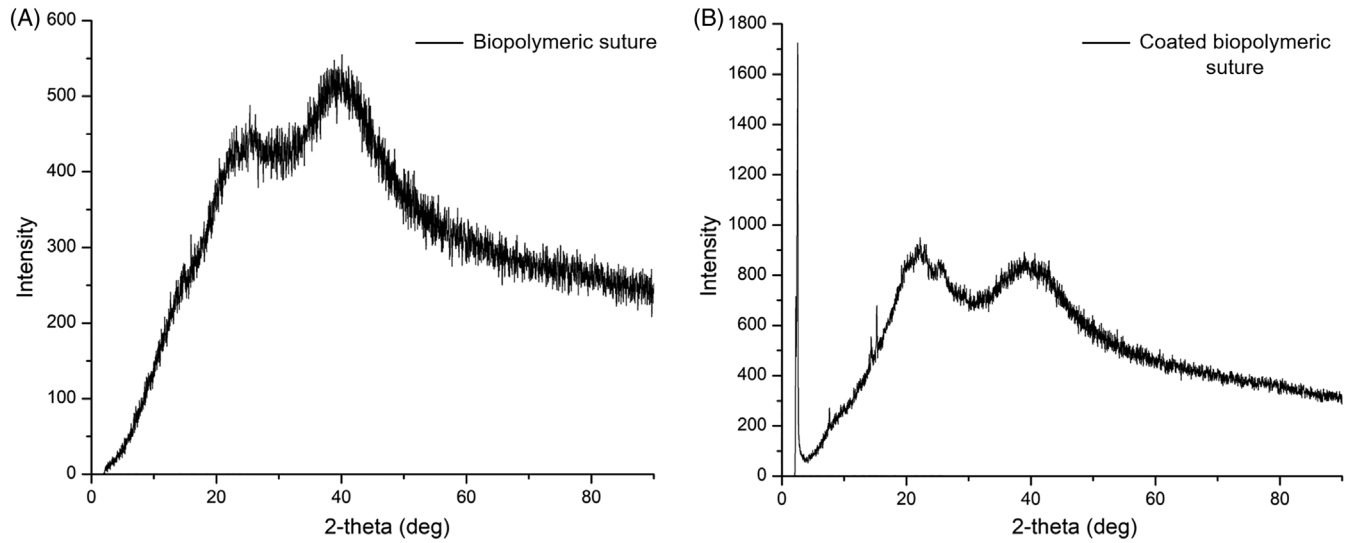

FIGURE 8 (A) X-ray diffraction pattern of the uncoated bioabsorbable suture and (B) of the coated bioabsorbable suture

which corresponds with the decomposition temperature indicated by the thermogravimetric analysis. The *thermogram* of the coated bioabsorbable suture did not reveal any new or additional information relative to the thermal analysis of individual biopolymers (Figure 9). The DSC curve of the bioabsorbable sutures closely resembled that of alginate, which also revealed two thermodynamic events—an endotherm

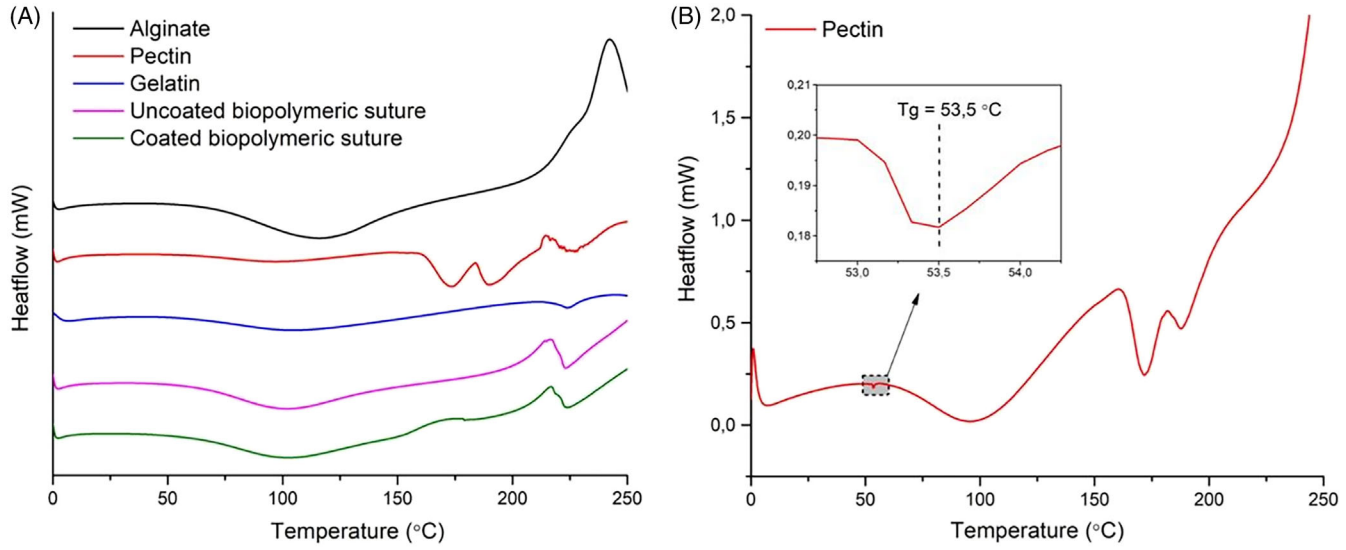

FIGURE 9 (A) DSC curve of the individual biopolymers, and the uncoated and coated bioabsorbable suture

around 100°C, that represents water evaporation and an exotherm around 240°C, that represents the decomposition of alginate.

Pectin displayed a similar endotherm and exotherm that corresponds with the weight loss events of water evaporation and decomposition, but also reveals three non-weight loss related peaks. These include a sudden deviation from the baseline at 53.5°C that represents the glass transition temperature of the polymer and two consecutive melting peaks at 172°C and 190°C, respectively. The DSC curve of gelatin also displayed an initial endotherm around 100°C that can be ascribed to water evaporation, followed by another endotherm at 222°C, that can be ascribed to the melting of the triple-helix crystalline structure of the polymer, as described by Shehap et al.[34] The melting peaks of pectin and gelatin was not observed in the DSC curve of the bioabsorbable suture, potentially because of the low concentration of the polymers in the final bioabsorbable suture formulation, or due to the interfering effect of the plasticizer and other constituents that disrupted the crystalline phases of the individual biopolymers.

3.1.5 | In vitro drug release of the lipid-drug coated bioabsorbable sutures

The in vitro release of DEX from coated bioabsorbable sutures was assessed at 37°C in PBS (pH 7.4) with continuous rotation as a simulation of physiological conditions. Prior to determining the release characteristics, the total amount of DEX loaded onto the coated bioabsorbable suture was determined via UV absorption at $\lambda = 241$ and normalized to bioabsorbable suture length (ug/cm). Dexamethasone is a fast-acting glucocorticoid with 26 times the anti-inflammatory potency of hydrocortisone. Hence, it is often used in low dosages of 500–2500 ug when applied topically or administered locally (e.g., 0.05%–0.25% dexamethasone creams, gels and eye-drops).[35] In the current study, 53ug of DEX was loaded per cm of bioabsorbable suture, indicating that a total amount of 1060 ug or 1 mg of DEX can be delivered with the use in 20 cm of bioabsorbable suture in vivo. This falls well within the normal clinical dosage range of DEX for localized delivery and suggest that effective anti-inflammatory activity can be achieved with the use of the coated bioabsorbable suture. Moreover, DEX is not considered to be cytotoxic and is administered in much higher dosages systemically (0.75–9 mg per day, depending on the condition being treated), confirming the safety of the loading dosage achieved in this study.

Figure 10 shows the cumulative concentration (ug/ml) and percentage of DEX released as a function of time, a duration of 1 week. An initial burst release was observed, whereby almost 70% of DEX was released within the first 24 h. A subsequent lag phase where the DEX release is almost zero order was then depicted and finally a linear phase from day 5, where the DEX release increased and started to resemble a first order release profile. Similar results have been observed for DEX-loaded PLGA particles.[36] We propose that DEX release in the current study, is governed by diffusion and dissolution of the drug and lipid layer as shown in Figure 10C. Initial burst release can be ascribed to the proximity of the drug to the bioabsorbable suture surface, the short distance of the diffusion layer and the high concentration gradient for DEX between the small lipid layer and the large volume of release medium. Another possible contributing factor to the movement of DEX away from the bioabsorbable suture surface, while the lipid layer still adheres to the bioabsorbable suture, as was observed macroscopically, is the relatively higher solubility of DEX (0.1 mg/ml) in PBS compared to the insolubility of soy phosphatidylcholine in aqueous media. This can also contribute to the following lag phase, where the concentration gradient is lower, the release media is more saturated and the lipophilic DEX prefers to remain within the lipid layer. However, after 5 days the lipid layer was observed to dissociate from the bioabsorbable suture surface, which potentially initiated the linear drug release phase by distributing into the release medium and increasing the surface area exposed. This dissociation

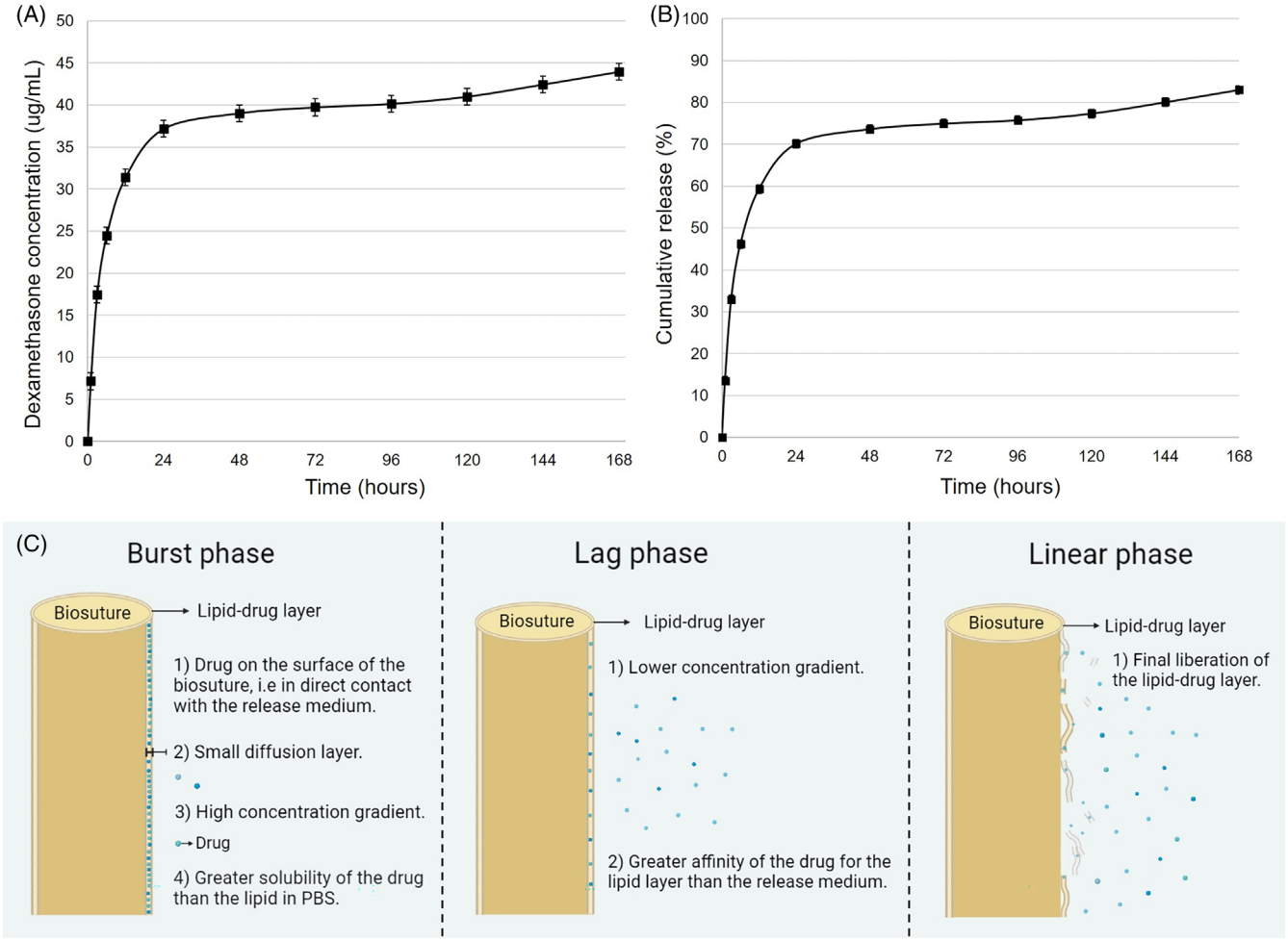

FIGURE 10 (A) Amount (ug/ml) of DEX released over a period of 7 days and (B) cumulative release (%) of DEX over a period of 7 days, both as normalized per cm of bioabsorbable suture and (C) graphical representation of the proposed mechanism of drug release from the coated bioabsorbable sutures. *Biosuture = bioabsorbable suture

was possibly triggered by the increased swelling of the bioabsorbable suture which made its surface more hydrophilic and served to repel the hydrophobic lipid layer.

The initial burst release of DEX will be valuable in preventing IRI, which occurs early after the restoration of blood flow, and in lessening the immediate inflammatory response that occurs in response to tissue damage. The continued release of DEX over a period of 7 days confirms the ability of the lipid layer to contain and retard the release of the drug, principally due to the good compatibility between lipophilic DEX and the lipid, SPC, as well as the low solubility of the lipid in an aqueous environment. Hence, with the coated bioabsorbable suture, protection against the occurrence of the no-reflow phenomenon, can also be obtained for approximately 7 days. Moreover, the lipid-based coating can serve to decrease the surface roughness of the bioabsorbable sutures by acting as a lubricating film and consequently reduce the mechanical stress during suturing. By the end of the drug release study, a proper 83% of the loaded drug was released and the linearity of the curve at this stage suggests that the remaining drug will be released over the next few days.

3.1.6 | Analysis of the in vitro swelling and degradation behavior of the bioabsorbable sutures

After crosslinking, polymeric hydrogels tend to no longer dissolve in aqueous media but rather swell upon immersion in ionic buffers. The swelling behavior is dependent on the inherent properties (e.g., hydrophilicity) and concentration of the polymers as well as known crosslinker factors, in regards to degree of crosslinking and or type of crosslinker agent.[37] In the current study, the uncoated and coated bioabsorbable sutures gradually swelled to reach an equilibrium swelling ratio of 9.213 and 8.741, respectively. It should be noted that the bioabsorbable sutures revealed no swelling upon immersion in pure distilled water, which indicates that the swelling behavior is governed by ionic interactions with ions, such as sodium (Na^+) in the employed buffer. As can be seen in Figure 9A, the coated bioabsorbable sutures swelled at a considerably slower pace that the uncoated bioabsorbable sutures, even though they both had similar final swelling ratios. This can be ascribed to the hydrophobic lipid-drug layer that covers the coated bioabsorbable suture and delays water absorption. The ends of the bioabsorbable sutures, where the samples were cut during

preparation, are however not covered by the hydrophobic layer, and allows water to freely penetrate the system, albeit at a much slower rate due to the small surface area that is exposed.

The overall swelling profiles of the bioabsorbable sutures are more gradual than what has previously been reported for other physically crosslinked alginate systems. Giz et al, for example, found that crosslinked alginate films swelled rapidly within the first 5 min of immersion in an aqueous media and reached equilibrium swelling after 50–60 min.[38] Similarly, alginate–pectin films prepared by Shahzad et al, swelled within 15 min and reached their swelling limit after 2 h.[39] Yet, these systems were all crosslinked with calcium as crosslinking ion, while in the current study we employed barium as crosslinking agent. According to Bajpai et al, the barium ion, which has a larger radius than calcium, fits securely in the polymer chain and does not undergo ion exchange as readily as other, smaller divalent cations.[40] This has been confirmed by Valentin et al, who found that alginate hydrogels that were crosslinked with Ba^{2+}, swelled and degraded much more slowly than those that were crosslinked with Ca^{2+} or Mg^{2+}.[41] The gradual swelling of the bioabsorbable sutures in the current study can, therefore, safely be ascribed to the large size if the barium ions that are tightly bound to the carboxyl groups of alginate and do not readily participate in the ion-exchange process.

The moderate swelling ratio of the coated and uncoated bioabsorbable sutures (9.213 and 8.699, respectively) is most probably a result of the type and concentration of both the biopolymers and crosslinkers employed. According to Li et al, crosslinking with 1.5% wt/vol calcium results in a fully crosslinked alginate system that provides significant resistance to swelling.[37] In the current study, barium, which has a greater ionic strength than calcium, was employed at 2% wt/vol, suggesting that the bioabsorbable suture system has a high crosslinking density and is aptly able to resist water penetration. Yet, alginate and gelatin are extremely hydrophilic polymers that are known to have high water absorption capacities, especially at the concentrations used in the current study.[39] Pectin, however, has been found to dramatically decrease the swelling capacity of gelatin films by forming strong electrostatic interactions with the polymer, which hinders the penetration of water molecules.[42] Hence, the specific combination of polymers and crosslinker used in the study, possibly resulted in equidistant swelling behavior where the high level of crosslinking largely prevented and stalled water penetration, but the hygroscopicity of the biopolymers ensured that sufficient swelling did take place. Furthermore, it should be noted that the swollen bioabsorbable sutures maintained their structural integrity with no signs of cracking or fracturing during the swelling process and remained easy to handle, even at their maximum swelling capacity. Additionally, the tensile strength of the swollen bioabsorbable sutures still adhered to the requirements of the United States Pharmacopeia, with a knot load failure of 2.01 *N* for the uncoated and 2.09 *N* for the coated bioabsorbable sutures, which is only slightly lower than the unswollen state. It should, however, be noted that the elongation at break of the bioabsorbable sutures in the swollen state increased to nearly 20%, due to the increased hydration and mobility of the polymer chains. This greater elasticity of the sutures allowed tighter and more secure knots to for, which is presumably the reason for the lack of a significant decrease in load failure and tensile strength values for the bioabsorbable sutures in the swollen state.

The degradation of the bioabsorbable sutures were studied over a period of 28 days, through incubation in PBS (pH = 7.4) at 37°C, rotating at 25 rpm to mimic physiological conditions and the results can be seen in Figure 11B. The degradation of alginate, pectin and gelatin systems are primarily based on hydrolysis and erosion mechanisms, while glycerol primarily diffuse out of the system as new areas are exposed to the aqueous media.[27] The human body does not produce the enzyme necessary to enzymatically degrade alginate and even though it does produce proteases (e.g., collagenase) that can degrade gelatin, several authors have found similar degradation rates for gelatin with or without collagenase, confirming a mainly hydrolytic degradation process for gelatin based systems.[43,44] In the current study, the uncoated and coated bioabsorbable sutures revealed similar degradation profiles, with the coated bioabsorbable sutures undergoing slightly less degradation, which is in accordance with the TGA results described earlier. The degradation profiles revealed an initial rapid weight loss within the first week, followed by a more gradual weight loss over the following weeks. By the end of the degradation study, that is, at day 28, the bioabsorbable sutures were almost completely degraded with only 20% of the original weight remaining. The first rapid weight loss phase corresponds well with literature and can be ascribed to loss of the lipid-drug layer from the bioabsorbable suture surface, leaching of the plasticizer out of the system as well as the easier removal of trapped water molecules after the swelling process.[45]

After the initial rapid weight loss in the first week, the bioabsorbable sutures continued to gradually degrade at a constant pace which can be ascribed to surface erosion due to hydrolytic degradation. In general, swellable polymer systems undergo one of two types of degradation processes—bulk erosion or surface erosion. Surface erosion occurs when the diffusion of water into the system is slower than the hydrolytic reactions and the water is used before it can reach the bulk of the system. This results in gradual and continuous degradation from the surface of the system, while bulk erosion is characterized by a period of no erosion followed by a sudden and spontaneous loss of weight and strength.[46] In the current study, SEM images of the bioabsorbable sutures during different time points of degradation, confirm surface degradation as the primary mechanism of degradation (Figure 11C). This form of degradation is ideal in suture materials where a sudden, rapid loss of suture material can lead to wound dehiscence and failure of the wound to heal.[47] However, gradual removal of the material from the bioabsorbable suture surface will provide continuous, diminishing support to the wound as it heals and regains its own strength. In Figure 11C, only a single, thin layer of the bioabsorbable suture remained after 28 days of incubation. This suggests that the bioabsorbable suture will be fully removed from the body shortly after the wound healing process is complete (approximately 2–3 weeks), thereby preventing unwanted irritation caused by the lengthy presence of a foreign body in the wound.

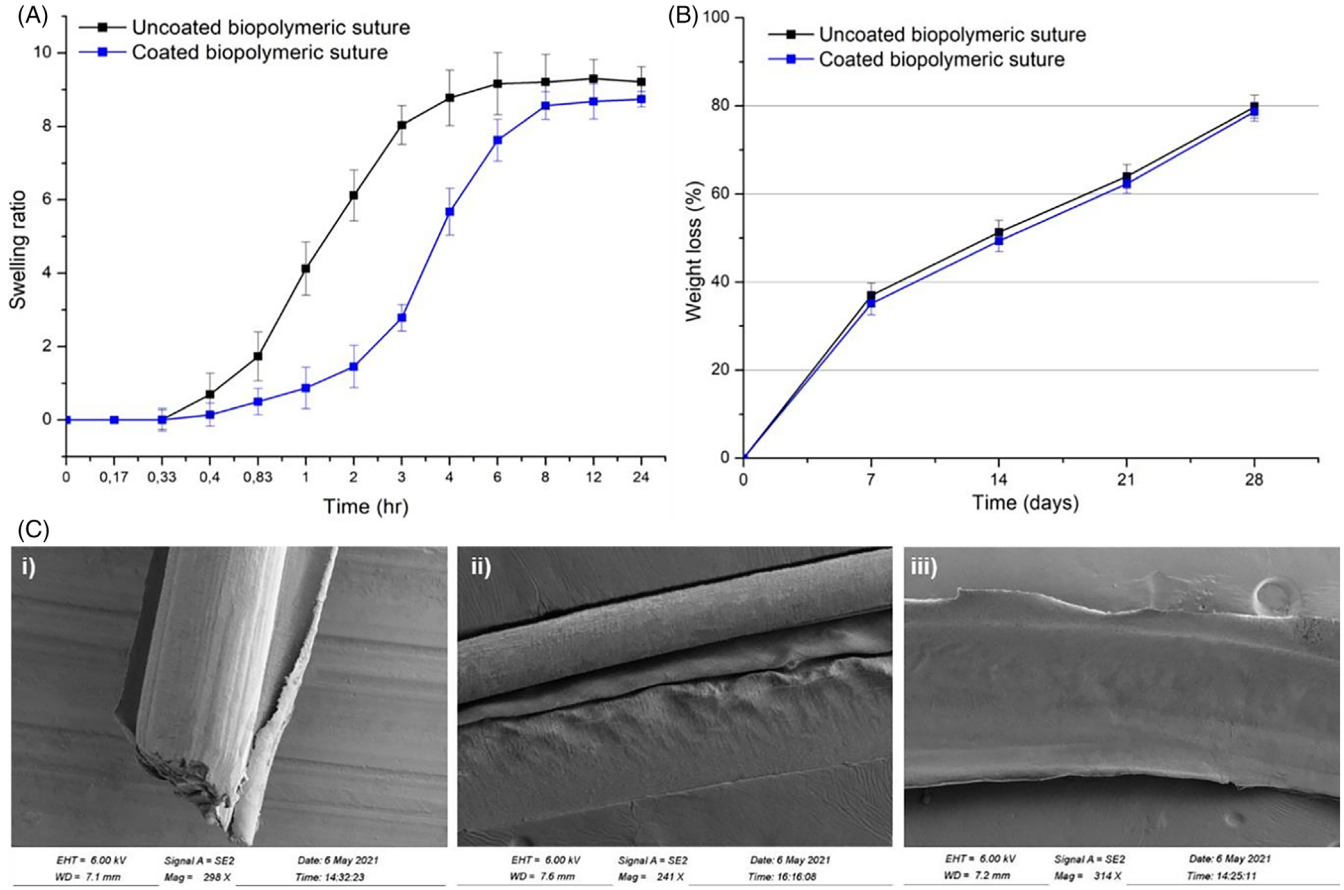

FIGURE 11 Swelling ratio (A) and degradation expressed as percentage weight loss (B) of the uncoated (black) and coated (blue) bioabsorbable sutures as a function of time immersed in phosphate buffered saline (pH = 7.4) at 37°C. (C) SEM images of bioabsorbable suture samples after 1 (i), 2 (ii) and 4 (iii) weeks of degradation

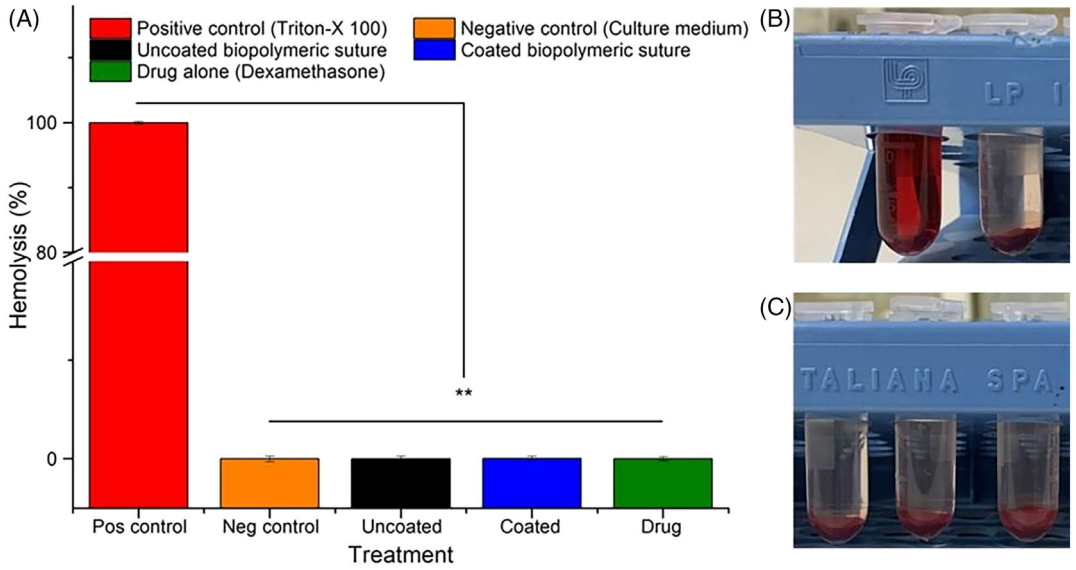

FIGURE 12 Hemocompatibility of the bioabsorbable sutures with (A) indicating the percentage haemolysis induced by each of the treatments; (B) showing the supernatant of the erythrocyte suspensions treated with the positive and negative control, representing 100% and 0% haemolysis respectively and (C) showing the supernatant of the suspensions treated, from left to right, with the uncoated bioabsorbable suture, the coated bioabsorbable suture and the drug

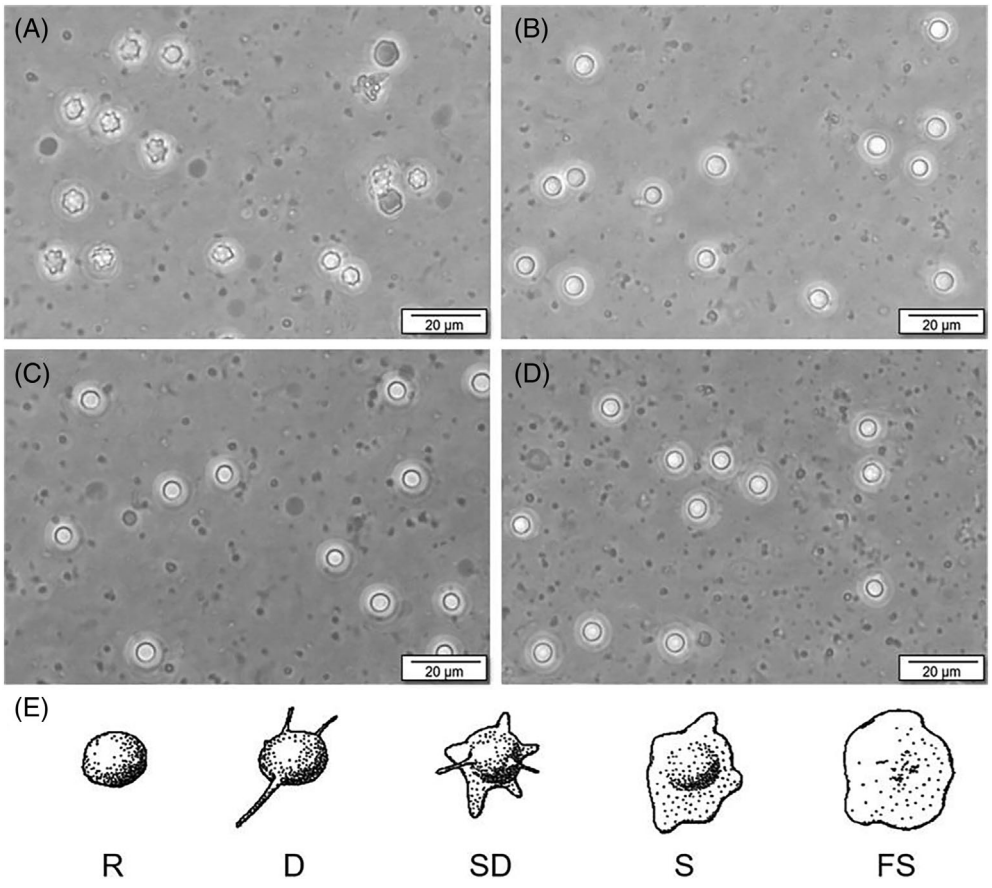

FIGURE 13 Platelet activation images after incubation with (A) positive control, (B) negative control, (C) uncoated bioabsorbable suture and (D) coated bioabsorbable suture. (E) Graphical representation (Reprinted with permission from Reference 52 Wiley copyright) of platelet activation stages, divided into five shape categories, from left to right, round or discoid (R), dendritic with early pseudopodia formation (D), spread dendritic with evident flattening (SD), spreading with early hyaloplasm (S), and fully spread with full hyaloplasm and no pseudopodia (FS)

3.1.7 | Analysis of the in vitro hemocompatibility of the bioabsorbable sutures

Hemocompatibility is an important component of biocompatibility, especially for biomaterials such as the current bioabsorbable suture, which will be in direct contact with the blood during in vivo clinical use.[48] Haemolysis provides a good indication of a biomaterial's compatibility with whole blood and has a permissible limit of 5%, for biomaterials to be considered hemocompatible.[49] The uncoated and coated bioabsorbable sutures displayed negligible haemolysis (<0.5%), as shown in Figure 12A, which was considerably lower than that of the positive control (100%) and that which has previously been reported for commercial PLLA sutures (4.75%).[50] This suggests that the bioabsorbable sutures, do not have a destructive effect on erythrocytes and can safely be used in procedures such as MVS, where the biomaterials will be in direct contact with whole blood.

Platelet activation is a critical step in the thrombus formation process and a key mechanism that confers biomaterial thrombogenicity. Platelet activation can easily be examined by categorizing platelet shapes into one of five known morphological forms, that is, round (R), dendritic with early pseudopodia formation (D), spread dendritic with evident flattening (SD), spreading with early hyaloplasm (S) and fully spread with full hyaloplasm and no pseudopodia (FS), that describe increasing platelet activation (Figure 13E).[51] The uncoated and coated bioabsorbable sutures, showed no indication of platelet activation with all platelets maintaining their original round or discoid morphology with no pseudopodia present (Figure 13C,D). The platelets treated with the positive control, on the other hand, showed clear signs of activation in the form of pseudopodia formation and spreading (Figure 13A). This provides a positive indication that the bioabsorbable sutures are not thrombogenic and will not encourage clotting when used in vivo.

3.1.8 | Analysis of the in vitro cytocompatibility of the bioabsorbable sutures

The biopolymers used in this study are known to have good biocompatibility, yet it remains imperative to confirm the safety and non-toxicity of the bioabsorbable sutures and their degradation products. In vitro cell studies can provide valuable information on the basic safety of novel biomaterials without the need for extravagant animal studies, which can be time consuming, costly, and lethal to the animals. According to the ISO 10993-5 standard, biomaterials can be classified as "biocompatible" if they result in an absolute minimum of 70% cell viability.[53] The uncoated and coated bioabsorbable sutures, however, only caused a slight decrease in cell viability of less than 5%, after 24 h of incubation. Additionally, after 48 h, the cell viability of the cells treated with the bioabsorbable suture extracts, was higher than the 100% viability achieved with the negative control (culture medium). This suggests that the bioabsorbable sutures supports and even encourages cell proliferation and

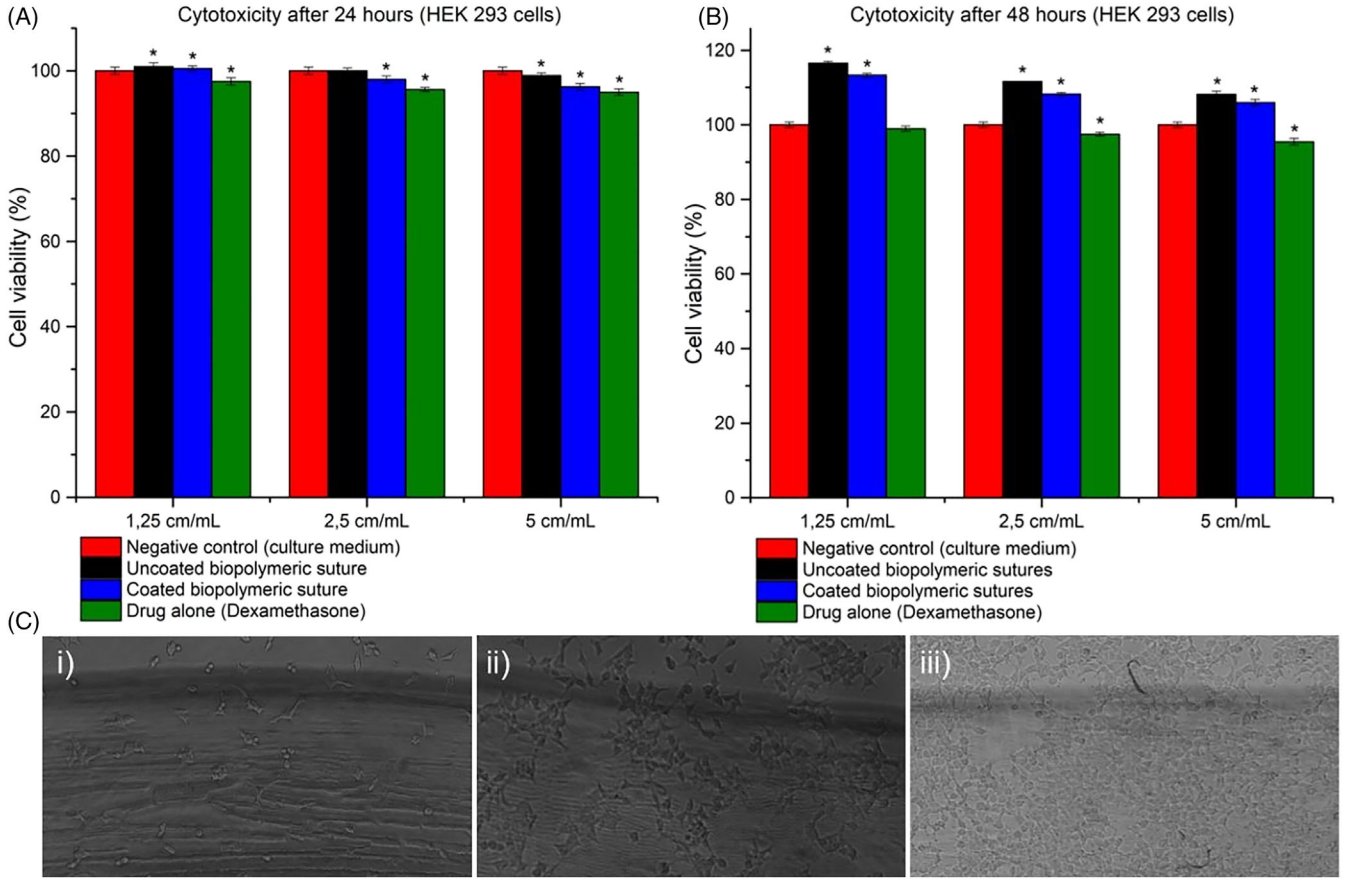

FIGURE 14 Cell viability of HEK 293 cells after 24 h (A) and 48 h (B); $p < .05$ indicated with (*); (C) light microscope images (×60 magnification) of the bioabsorbable sutures, showing cell attachment after (i) 12 h, (ii) 24 h and (iii) 48 h of incubation

is in agreement with the results of other researchers, who found that natural polymers, such as alginate and gelatin, stimulate cell growth and allows for faster wound healing.[51]

The cell viability of the coated bioabsorbable sutures was slightly lower than that of the uncoated bioabsorbable sutures, which can be ascribed to the presence of the drug, dexamethasone, in the coating. Dexamethasone is known to be cytotoxic to certain cell types, such as osteoblasts, and was found to decrease the viability of HEK 293 cells in the current study (Figure 14A,B).[54] Yet, the coated bioabsorbable suture still managed to encourage cell proliferation and can be considered as safe and biocompatible. This is further confirmed by light microscope images of the cells after incubation with segments of the bioabsorbable sutures (Figure 14C). These images confirm that the cells are able to comfortably proliferate on the surface of the bioabsorbable sutures and supports the notion that the RDG peptide sequence in biopolymers such as gelatin, allows for effective interaction between cells and biomaterials.

4 | CONCLUSIONS

In this work, a novel bioabsorbable suture material consisting of natural biopolymers was fabricated and coated with a lipid-drug layer for sustained, localized drug release. The bioabsorbable sutures displayed impressive mechanical properties that exceeded the US Pharmacopoeia's guidelines for minimum knot strength, which suggests that the bioabsorbable sutures will serve as effective clinical counterpart to the synthetic sutures that are currently on the market. The bioabsorbable sutures were characterized by multiple approaches including FTIR, and DSC, among others. Analysis of the surface morphology of the bioabsorbable sutures revealed a smooth, uniform surface topography that should allow the bioabsorbable suture to easily glide through tissues without causing unwanted sawing and damage. The drug release profile revealed sustained DEX release over a period of 7 days with an initial burst release phase, followed by a lag phase and a final linear phase. This release profile is suitable for the prevention of IRI after microvascular surgery where immediate, yet sustained anti-inflammatory action is needed, as well as no-reflow, where extended protection is required. Degradation of the bioabsorbable sutures took place over a period of 28 days through surface erosion and hydrolytic degradation. This form of degradation is highly desirable in suture materials and suggests that the bioabsorbable suture will gradually lose strength as the wound heals and regains its own strength. The bioabsorbable sutures displayed excellent biocompatibility with no sighs of cytotoxicity or inducing haemolysis and platelet activation. The results reported in this study provide information on a

novel, monofilament, absorbable, drug-eluting bioabsorbable suture that, if it reaches the clinical market, can drastically improve microvascular surgery outcomes and decrease the severity and occurrence of IRI and no-reflow after microvascular anastomosis. The obtained results justify further development of the bioabsorbable suture, however studies to account for the long-term stability should be conducted. Further studies will be conducted to determine the angiogenic capacity and in vivo efficacy of the bioabsorbable suture.

ACKNOWLEDGEMENTS

This work was supported by the National research Foundation (NRF) of South Africa: SARChI and CSRP.

CONFLICT OF INTEREST

The authors declare no conflict of interest.

AUTHOR CONTRIBUTIONS

Conceptualization: Yahya E. Choonara, Thashree Marimuthu, Pierre P. D. Kondiah and Pradeep Kumar. *Methodology*: Yahya E. Choonara, Thashree Marimuthu, Pierre P. D. Kondiah, Pradeep Kumar and Kara M. de la Harpe. *Data collection and analysis*: Philemon Ubanako and Kara M. de la Harpe. *Writing-original draft preparation*: Yahya E. Choonara, Thashree Marimuthu, Pierre P. D. Kondiah, Pradeep Kumar and Kara M. de la Harpe. *Writing-review & editing*: Yahya E. Choonara, Thashree Marimuthu, Pierre P. D. Kondiah, Pradeep Kumar and Kara M. de la Harpe. *Supervision*: Yahya E. Choonara, Thashree Marimuthu, and Pierre P. D. Kondiah. *Funding acquisition*: Yahya E. Choonara, Thashree Marimuthu, Pierre P. D. Kondiah and Pradeep Kumar.

DATA AVAILABILITY STATEMENT

The data that support the findings of this study are available from the corresponding author upon reasonable request.

ORCID

Kara M. de la Harpe https://orcid.org/0000-0001-8171-3296
Thashree Marimuthu https://orcid.org/0000-0003-1487-5273
Pierre P. D. Kondiah https://orcid.org/0000-0002-5113-8507
Pradeep Kumar https://orcid.org/0000-0002-8640-4350
Yahya E. Choonara https://orcid.org/0000-0002-3889-1529

REFERENCES

1. Samadian H, Maleki H, Allahyari Z, Jaymand M. Natural polymers-based light-induced hydrogels: promising biomaterials for biomedical applications. *Coord Chem Rev*. 2020;420:213432.
2. Deng X, Qasim M, Ali A. Engineering and polymeric composition of drug-eluting suture: a review. *J Biomed Mater Res - Part A*. 2021;109(10):2065-2081.
3. Abhari RE, Martins JA, Morris HL, Mouthuy PA, Carr A. Synthetic sutures: clinical evaluation and future developments. *J Biomater Appl*. 2017;32(3):410-421.
4. Kumaran SK, Chopra M, Oh E, Choi H-J. Biopolymers and natural polymers. In Narain R, ed. *Polymer Science and Nanotechnology*. Elsevier Inc.; 2020;245-256.
5. Varaprasad K, Jayaramudu T, Kanikireddy V, Toro C, Sadiku ER. Alginate-based composite materials for wound dressing application:a mini review. *Carbohydr Polym*. 2020;236:116025.
6. Dott C, Tyagi C, Tomar LK, Choonara YE, Kumar P, du Toit LCPV. A mucoadhesive electrospun nanofibrous matrix for rapid oramucosal drug delivery. *J Nanomater*. 2013;924947:1-19.
7. Bello AB, Kim D, Kim D, Park H, Lee SH. Engineering and functionalization of gelatin biomaterials: from cell culture to medical applications. *Tissue Eng - Part B Rev*. 2020;26(2):164-180.
8. Afewerki S, Sheikhi A, Kannan S, Ahadian S, Khademhosseini A. Gelatin-polysaccharide composite scaffolds for 3D cell culture and tissue engineering: towards natural therapeutics. *Bioeng Transl Med*. 2019;4(1):96-115.
9. Wang WZ, Baynosa RC, Zamboni WA. Update on ischemia-reperfusion injury for the plastic surgeon. *Plast Reconstr Surg*. 2011;128(6):685-692.
10. Bouleti C, Mewton N, Germain S. The no-reflow phenomenon: state of the art. Arch. *Cardiovasc. Dis*. 2015;108(12):661-674.
11. Johnson EO, Vekris MD, Zoubos AB, Soucacos PN. Neuroanatomy of the brachial plexus: the missing link in the continuity between the central and peripheral nervous systems. *Off. J. Int. Microsurg. Soc. Eur. Fed. Soc. Microsurg*. 2006;26(4):218-229.
12. Byvaltsev VA, Akshulakov SK, Polkin RA, et al. Microvascular anastomosis training in neurosurgery: a review. *Minim Invasive Surg*. 2018;2018:1-9.
13. Leaper DJ, Edmiston CE, Holy CE. Meta-analysis of the potential economic impact following introduction of absorbable antimicrobial sutures. *Br J Surg*. 2017;104(2):e134-e144.
14. Sánchez-Hernández CD, Torres-Alarcón LA, González-Cortés A, Peón AN, Rungatscher A. Ischemia/reperfusion injury: pathophysiology, current clinical management, and potential preventive approaches. *Mediators Inflamm*. 2020;2020:8405370.
15. Hu C, Lu W, Mata A, Nishinari K, Fang Y. Ions-induced gelation of alginate: mechanisms and applications. *Int J Biol Macromol*. 2021;177:578-588.
16. Obermeier A, Schneider J, Föhr P, et al. In vitro evaluation of novel antimicrobial coatings for surgical sutures using octenidine. *BMC Microbiol*. 2015;15(1):1-8.
17. NF 24 U 29. *Unites States Pharmacopoeia (USP) Monograph: Absorbable Surgical Suture*. The United States Pharmacopeial Convention Inc.; Rockville (MD); 2007:2050.
18. Jung F, Braune S, Lendlein A. Haemocompatibility testing of biomaterials using human platelets. *Clin Hemorheol Microcirc*. 2013;53(1–2):97-115.
19. Sunitha S, Adinarayana K, Sravanthi RP, et al. Fabrication of surgical sutures coated with curcumin loaded gold nanoparticles. *Pharm Anal Acta*. 2017;8(529):2.
20. Von Fraunhofer JA. Mechanical properties. In: Chu C-C, von Fraunhofer JA, Greisler HP, eds. *Wound Closure Biomaterials and Devices*. CRC Press; 2018:107-130.
21. Thom D, Dea IC, Morris ERPD. Interchain associations of alginate and pectins. *Prog Food Nutr Sci*. 1982;6(1–6):97-108.
22. Bierhalz ACK, Da Silva MA, Kieckbusch TG. Natamycin release from alginate/pectin films for food packaging applications. *J Food Eng*. 2012;110(1):18-25.
23. Lambrech MVP, Sorrivas V, Villar MA, Lozano JE. Structure and permeability of low-methoxyl pectin (LMP)-sodium alginates (NaAlg) films. *Chem Eng Trans*. 2009;17(8000):1765-1770.
24. Gohil RM. Synergistic blends of natural polymers, pectin and sodium alginate. *J Appl Polym Sci*. 2011;120(4):2324-2336.
25. Walkenström P, Kidman S, Hermansson AM, Rasmussen PB, Hoegh L. Microstructure and rheological behaviour of alginate/pectin mixed gels. *Food Hydrocoll*. 2003;17(5):593-603.
26. Taira N, Ino K, Robert J, Shiku H. Electrochemical printing of calcium alginate / gelatin hydrogel. *Electrochim Acta*. 2018;281:429-436.
27. Wang QQ, Liu Y, Zhang CJ, Zhang C, Zhu P. Alginate/gelatin blended hydrogel fibers cross-linked by Ca^{2+} and oxidized starch: preparation and properties. *Mater Sci Eng C*. 2019;99:1469-1476.

28. Sirviö JA, Visanko M, Ukkola J, Liimatainen H. Effect of plasticizers on the mechanical and thermomechanical properties of cellulose-based biocomposite films. *Ind Crops Prod*. 2018;122:513-521.
29. Gao C, Pollet E, Avérous L. Properties of glycerol-plasticized alginate films obtained by thermo-mechanical mixing. *Food Hydrocoll*. 2017;63:414-420.
30. Della Porta G, Del Gaudio P, De Cicco F, Aquino RP, Reverchon E. Supercritical drying of alginate beads for the development of aerogel biomaterials: optimization of process parameters and exchange solvents. *Ind Eng Chem Res*. 2013;52(34):12003-12009.
31. Guambo MPR, Spencer L, Vispo NS, et al. Natural cellulose fibers for surgical suture applications. *Polymers (Basel)*. 2020;12(12):1-20.
32. Awasthi R, Kulkarni GT, Ramana MV, et al. Dual crosslinked pectin–alginate network as sustained release hydrophilic matrix for repaglinide. *Int J Biol Macromol*. 2017;97:721-732.
33. Johnston D, Choonara YE, Kumar P, Du Toit LC, Van Vuuren S, Pillay V. Prolonged delivery of ciprofloxacin and diclofenac sodium from a polymeric fibre device for the treatment of peridontal disease. *Biomed Res Int*. 2013;2013:1-15.
34. Shehap AM, Mahmoud KH, Abd El-Kader MFH, El-Basheer TM. Preparation and thermal properties of gelatin/TGS composite films. *Middle East J Appl Sci*. 2015;5(1):157-170.
35. Nussenblatt RB. *Philosophy, Goals, and Approaches to Medical Therapy in Uveitis Fundamentals and Clinical Practice*. Mosby; 2010:76-113.
36. Lee DH, Kwon TY, Kim KH, et al. Anti-inflammatory drug releasing absorbable surgical sutures using poly(lactic-co-glycolic acid) particle carriers. *Polym Bull*. 2014;71(8):1933-1946.
37. Li J, Wu Y, He J, Huang Y. A new insight to the effect of calcium concentration on gelation process and physical properties of alginate films. *J Mater Sci*. 2016;51(12):5791-5801.
38. Giz AS, Berberoglu M, Bener S, et al. A detailed investigation of the effect of calcium crosslinking and glycerol plasticizing on the physical properties of alginate films. *Int J Biol Macromol*. 2020;148:49-55.
39. Shahzad A, Khan A, Afzal Z, Umer MF, Khan J, Khan GM. Formulation development and characterization of cefazolin nanoparticles-loaded cross-linked films of sodium alginate and pectin as wound dressings. *Int J Biol Macromol*. 2019;124:255-269.
40. Bajpai SK, Sharma S. Investigation of swelling/degradation behaviour of alginate beads crosslinked with Ca^{2+} and Ba^{2+} ions. *React Funct Polym*. 2004;59(2):129-140.
41. Valentin TM, Leggett SE, Chen PY, et al. Stereolithographic printing of ionically-crosslinked alginate hydrogels for degradable biomaterials and microfluidics. *Lab Chip*. 2017;17(20):3474-3488.
42. Farris S, Schaich KM, Liu LS, Cooke PH, Piergiovanni L, Yam KL. Gelatin-pectin composite films from polyion-complex hydrogels. *Food Hydrocoll*. 2011;25(1):61-70.
43. Rosellini E, Cristallini C, Barbani N, Vozzi G, Giusti P. Preparation and characterization of alginate/gelatin blend films for cardiac tissue engineering. *J Biomed Mater Res - Part A*. 2009;91(2):447-453.
44. Van Den Bosch E, Gielens C. Gelatin degradation at elevated temperature. *Int J Biol Macromol*. 2003;32(3–5):129-138.
45. Li D, Li P, Zang J, Liu J. Enhanced hemostatic performance of tranexamic acid-loaded chitosan/alginate composite microparticles. *J Biomed Biotechnol*. 2012;2012:1-9.
46. Schedl L. Why degradable polymers undergo surface erosion or bulk erosion. *Biomaterials*. 2002;23:4221-4231.
47. Goel A. Surgical sutures—a review. *Delhi J Ophthalmol*. 2016;26(3):159-162.
48. de la Harpe KM, Kondiah PP, Choonara YE, Marimuthu T, du Toit LC, Pillay V. The hemocompatibility of nanoparticles: a review of cell–nanoparticle interactions and hemostasis. *Cell*. 2019;8(1209):1-25.
49. Kandimalla R, Kalita S, Choudhury B, et al. Fiber from ramie plant (Boehmeria nivea): a novel suture biomaterial. *Mater Sci Eng C*. 2016;62:816-822.
50. Hu W, Huang ZM, Meng SY, He CL. Fabrication and characterization of chitosan coated braided PLLA wire using aligned electrospun fibers. *J Mater Sci Mater Med*. 2009;20(11):2275-2284.
51. Chiaoprakobkij N, Seetabhawang S, Sanchavanakit N, Phisalaphong M. Fabrication and characterization of novel bacterial cellulose/alginate/gelatin biocomposite film. *J Biomater Sci Polym Ed*. 2019;30(11):961-982.
52. Goodman SL. Sheep, pig, and human platelet-material interactions with model cardiovascular biomaterials. *J Biomed Mater Res*. 1999;45(3):240-250.
53. Chen X, Hou D, Wang L, Zhang Q, Zou J, Sun G. Antibacterial surgical silk sutures using a high-performance slow-eelease carrier coating system. *ACS Appl Mater Interfaces*. 2015;7(40):22394-22403.
54. Zhu C-Y, Yao C, Zhu l-q, She C, Zhon ZX. Dexamethasone-induced cytotoxicity in human osteoblasts is associated with circular RNA HIPK3 downregulation. *Biochem Biophys Res Commun*. 2019;516(3):645-652.

SUPPORTING INFORMATION

Additional supporting information may be found in the online version of the article at the publisher's website.

How to cite this article: de la Harpe KM, Marimuthu T, Kondiah PPD, Kumar P, Ubanako P, Choonara YE. Synthesis of a novel monofilament bioabsorbable suture for biomedical applications. *J Biomed Mater Res*. 2022;110(10):2189-2210. doi:10.1002/jbm.b.35069